

LA-8314-PR
Progress Report

UC-92
Issued: December 1980

Remote Characterization of Fluid Saturation in Western Sands

April 1, 1979—March 31, 1980

Ernest B. Nuckols
Jasper A. Jackson



CONTENTS

LIST OF ILLUSTRATIONS	iv
LIST OF TABLES	vi
ABSTRACT	1
I. INTRODUCTION	2
II. BACKGROUND	3
III. WGS RESEARCH AT LASL	6
A. Task 1: Permeability and Porosity Studies on Core Samples	7
B. Task 2: Geological support Studies	9
C. Task 3: Nuclear Magnetic Resonance Studies	9
1. Theoretical Studies	10
IV. LABORATORY STUDIES: DETECTION OF NUCLEAR MAGNETIC RESONANCE IN A REMOTELY PRODUCED REGION OF HOMOGENEOUS MAGNETIC FIELD	22
A. The Experiments	22
1. Toroidal Region of Homogeneous Magnetic Field	22
2. NMR Spectrometer	25
B. Results	29
V. SENSITIVITY OF NMR DETECTION FOR EXTERNAL SAMPLES	36
A. The Experiments	36
B. Results and Discussion	37
VI. PROTOTYPE DOWNHOLE TOOL DEVELOPMENT	45
VII. PROJECTED IMPROVEMENTS	48
VIII. SUMMARY FY 79 ACCOMPLISHMENTS IN NMR	51
REFERENCES	52

LIST OF ILLUSTRATIONS

Fig. No.

- | | |
|--|----|
| 1. Magnetic field of opposed current loops. | 11 |
| 2. Three-dimensional plot of H_r vs (h/a) and H_r vs (r/a) . | 13 |

3.	Variation of the H_r/H_0 vs r for two opposed infinite solenoids of radius a .	14
4.	Variation of peak H_r vs separation of field producing elements (loops or solenoids).	15
5.	Variation of homogeneous field width (r/a) in midplane for $H_r/H_0 = 100$ ppm.	16
6.	Variation of (H_r/H_0) with distance from midplane ($z = 0$) for 4 inch ($a = 5.08$ cm) diameter magnets and 1 foot separation ($h/a = 3$).	17
7.	Measured H_r for two 3 inch square permanent magnets (6 inch long) as a function of radial distance from magnet edge.	19
8.	Measured values of peak positions and field for two 3 inch square permanent magnets.	20
9.	Calculated variation of peak field for finite length magnets as a function of length. (For $a = 5.08$ cm and $h/a = 3$).	21
10.	Magnet configuration for production of toroidal region of homogeneous radial magnetic field.	23
11.	Upper - D.C. magnetic field plot showing homogeneous region. Lower - rf magnetic field vs distance from coil.	24
12.	Production of 90° pulse by rf field at toroidal region of homogeneous magnetic field.	26
13.	Induction of voltage in rf coil by precessing nuclear magnetization following 90° rf pulse.	27
14.	Glycerol-filled pyrex annulus mounted at $r = 14$ cm in midplane of magnet.	30
15.	Proton NMR signal from glycerol-filled tygon torus at $r = 14$ cm.	31
16.	Glycerol-filled styrofoam tub surrounding rf coil in magnet midplane.	32
17.	Proton NMR signal from the homogeneous toroidal region in a glycerol-filled tub at $r = 14$ cm.	33
18.	Geometry of the cylindrically symmetric external samples.	38
19.	Plot of the relative signal per unit volume g (+) and the rf pulse length (X) versus (R/a) .	39
20.	Plot of the relative signal per unit volume as a function of $(a/R)^3$. The solid line is the prediction of Equation (4).	43

21. Projected performance of logging tool using superconducting magnets.	46
22. Calculated integration time to achieve given S/N at selected depth into formation utilizing optimized electronics and superconducting magnets.	49

LIST OF TABLES

Table No.

I. Radial Dimensions of the Annular Samples	40
---	----

REMOTE CHARACTERIZATION OF FLUID SATURATION
IN WESTERN SANDS

April 1, 1979 - March 31, 1980

by

Ernest B. Nuckols and Jasper A. Jackson

ABSTRACT

The Department of Energy has placed major emphasis on enhanced gas production, of which the Western Gas Sands (WGS) is one of four unconventional resources that is being studied. Research at the Los Alamos Scientific Laboratory is aimed at the development of methods to define fluid saturation, porosity, and permeability in WGS as found under in situ reservoir conditions. These analyses are being coordinated with nuclear magnetic resonance (NMR) studies, which will lead ultimately to the design of an improved downhole NMR tool.

I. INTRODUCTION

The Department of Energy has placed major emphasis on enhanced gas production, of which the Western Gas Sands (WGS) is one of four unconventional resources that is being studied intensively. Approximately 24 major basins in the western US are known to contain gas-bearing sand lenses. Significant gas production has occurred from several of these basins during the last 30 years, but the last 10 years has seen a marked production decline. This production decline has increased even though novel and routine stimulating techniques have been employed.

In the past, routine geophysical log analysis has not been definitive, so comparisons of complete log suites from producing and dry holes show few discernible differences. Log and core analyses have shown that fluid saturations are of primary interest, with typical producing formations having relatively low porosities. With such low porosity, conventional geophysical logging tools are not useful. Therefore, Los Alamos Scientific Laboratory (LASL) has concentrated on new concepts to measure fluid saturations.

Initial work has centered on the use of nuclear magnetic resonance (NMR). NMR techniques measure the precession of a magnetic moment in an applied field. Earlier work was limited by the weak natural magnetic field of the earth and the fact that the measurement and corresponding magnetic fields were limited to the neighborhood of the wellbore. LASL has developed new NMR approaches that permit measurements of the concentration and type of nuclei at a distance from the wellbore.

These techniques, as now conceived, will be useful to measure proton concentrations at discrete distances from the side of a wellbore. Consequently, these techniques will also be useful to measure fluid invasion distances and rates.

II. BACKGROUND

Nuclear Magnetic Logging was introduced in the mid-50's and was recognized as having a unique potential for reservoir evaluation in the petroleum industry. In particular, it was the only technique that could determine properties of fluid in the pores of geological reservoirs because it looked directly (and only) at the fluid. For example, it is potentially capable of measuring the producible oil in place (the Free Fluid Index). Relaxation times of the nuclei of the atoms in the fluid (oil) were found to be inversely related to the size of the pore containing the fluid. This was found to be the case when fluid molecules in contact with the pore walls are influenced by relaxation mechanisms not felt by the nuclei of molecules in bulk fluid. It was learned that as the pore size decreased, bulk molecules have an increasing chance to diffuse to the wall before they relax at their undisturbed (bulk) rate.

The above phenomena were confirmed in extensive laboratory tests. The petroleum industry, however, encountered difficulties in making reliable field measurements. Prominent among these was the problem of an overwhelming signal from the water protons in the drilling mud, both in the drill hole and in the formation where drilling mud had invaded.

The present commercial technique, and, apparently, all past field experience, involves using a coil or solenoid to establish a strong direct current magnetic field in the formation near the borehole. This field tends to produce a net magnetization of the nuclear magnetic moments in the formation fluid at some angle to the earth's magnetic field. After maintaining the direct current field for a time sufficient for the nuclear magnetization to reach equilibrium, the field is turned off rapidly (with respect to the nuclear magnetization

time) and the previously established magnetization precesses about the earth's field at the Larmor frequency appropriate for that field strength of the earth.

However, there are several difficulties with this system. First, the direct current field is strongest near the tool and thus the magnetization produced will be strongest there; i.e., in the fluid in the borehole rather than further out in the formation where the fluid of interest is located. Second, the signal will be rather weak because of the low frequency of precession in the weak field of the earth. Elaborate and costly drilling treatment procedures have been developed (e.g., adding magnetite to extinguish the signal from the borehole fluids and adding organic paramagnetic ions to extinguish the signal from the invaded zones of the formation) for circumventing these problems. A third limitation on the presently available systems is the ~10 to 20-ms dead time after the field is turned off before a signal from the precessing nuclei can be detected. This has limited its use to formations with relatively large porosity and permeability.

The desirability of developing an alternate logging procedure has long been recognized and many schemes are cited in the patent literature. It is believed that few, if any, have been promising enough to test in the laboratory, and obviously, none have been reduced to practice. However, NMR techniques have undergone a revolution in sophistication in the last 10 years and it is now desirable to investigate the possibility that there might be a new approach that would prove fruitful. The present work at LASL was prompted after observing first hand the logging of a hole and witnessing the time-consuming preparation necessary to "kill" the borehole and invaded zone(s) fluid signals. At LASL, a program is under way to examine the possibility of using direct current and radio frequency magnetic fields produced by sources

in the borehole to produce a magnetic resonance at any arbitrary distance from the borehole.

III. WGS RESEARCH AT LASL

The purpose of this research is to develop methods to define fluid saturation, porosity, and permeability in WGS as found under in situ reservoir conditions. These analyses will then be correlated with nuclear magnetic resonance studies that will lead ultimately to the design of an improved downhole NMR tool. During FY 79, work was initiated to respond to these research activities. The three main task areas were:

- Task 1: Permeability and Porosity Studies on Core Samples,
- Task 2: Geological Support Studies, and
- Task 3: Nuclear Magnetic Resonance Studies.

A. Task 1: Permeability and Porosity Studies on Core Samples

During the past year, a complete laboratory was set up and an experimental program was designed to address the objectives of this task. These goals, which are complementary to our central NMR investigation, are to be able to routinely measure porosity and permeability (nano-Darcy range) of synthetic and natural core samples employed in NMR studies and to possess the capability to investigate the effects of such variables as microscale structure, temperature, pressure, water saturation, and pore throat obstruction on the bulk porosity and permeability of these samples. It is believed that by elucidating the physical microstructure of various lithologies, as well as their response to varying conditions of temperature, fluid saturation, pressure, etc., improved information can be obtained for the developing NMR tool. Then, ultimately, the macroscale behavior of fluids in formations of interest can be better understood, predicted, and controlled.

Laboratory equipment acquired to date includes sample preparation equipment (for both macro- and microsamples), a 15,000-psi porosimeter apparatus for measuring nano-Darcy permeabilities of core samples to both liquids and gases under variable hydrostatic pressures up to 5000 psi, and scanning electron and various optical microscopes to be used in microstructural investigations.

Some initial measurements made on a sample from the Twin Arrow Well in the Piceance Basin of Colorado were:

<u>Depth (ft.)</u>	<u>Porosity</u>	<u>Permeability (wet)</u>	<u>Permeability (Dry)</u>
1010	*	\geq .01 millidarcy	~ .0013 millidarcy
1014	*	\geq .01 millidarcy	~ .03 - .04 millidarcy

* not measured

In addition, the response of a core from a Pacific Transmission Supply Company well (No. 3-10-A) in Sweetwater County, Wyoming, to variable confining pressures was measured as below:

<u>Confining Pressure (PSIA - 20 minutes)</u>	<u>Permeability in Millidarcy +S.D% (6404.0 ft.)</u>
200	.674 <u>±</u> 0.6%
400	.488 <u>±</u> 0.6%
600	.422 <u>±</u> 0.8%
800	.386 <u>±</u> 3.0%
0000	.348 <u>±</u> 2.2%
0200	.327 <u>±</u> 2.5%
0400	.299 <u>±</u> 0.0%
0600	.280 <u>±</u> 0.6%
0800	.270 <u>±</u> 3.0%
2000	.254 <u>±</u> 0.7%
2200	.246 <u>±</u> 0.7%
2400	.237 <u>±</u> 0.7%
2600	.277 <u>±</u> 0.3%
2800	.222 <u>±</u> 0.0%
3000	Not Tested

Additional capabilities of the porosity/permeability laboratory include the ability to determine virtual and real core density and pore-size distributions for those pores with throat diameters as small as 120 Å. From this information, data on connected-pore surface areas can be obtained and estimates of the distribution of pore throat radii can be made. This type of information will prove to be critical in any attempt to understand the relative importance of flow through a rock's porous fabric vs flow along fracture channels.

Another apparatus is also available for analyzing triaxial dilation (or contraction), and changes in liquid/gas permeabilities as core specimens are subjected to varying conditions of temperature and pressure.

When combined with the above investigations, a systematic study of the microstructure of tight gas sands reservoir lithologies utilizing scanning electron and optical microscopy should aid in elucidating the relationship between rock microstructure and the porosity and permeability (or lack thereof) in a typical WGS formation. Investigations with the scanning electron microscope (SEM) will include pore geometry and connected-pore characterization, and correlation of microstructural lithologic features (intergranular recrystallization, pore throat obstruction by micro particles, etc.) with the bulk permeability and porosity of core samples. Optical methods should provide us with information regarding depositional environment, lithologic texture, mineralogy, post-depositional lithification and/or dissolution features, and various other parameters that should aid in understanding the structure of fluid flow pathways in porous rock fabrics.

All of these studies are designed to enhance our ability to design a workable porosity/permeability NMR tool by providing pertinent information on how fluids are incorporated in, interact with, and are transported through a tight gas sand reservoir.

B. Task 2: Geological Support Studies

Activities in this task area of comparing laboratory measurements against existing geophysical log suites and core descriptions were temporarily delayed until more extensive laboratory work could be accomplished.

C. Task 3: Nuclear Magnetic Resonance Studies

FY 79 efforts in nuclear magnetic resonance studies have been concentrated:

- Theoretical Studies,
- Laboratory Studies, and
- Downhole Prototype Tool Development.

1. Theoretical Studies. Remote production of a region of homogeneous magnetic field can be accomplished by two simple methods. Both are based on the following principle. If two equal field sources are arranged axially so their fields oppose in the region between them, then there exists a region near the plane perpendicular to the axis midway between the sources where H_r , the radial component of the field, goes through a maximum. Near the maximum, the field is homogeneous to within any chosen degree over prescribed regions.

a. Field of Opposing Current Loops. Consider a pair of coils arranged as shown in Fig. 1, with spacing $2h$ and radius a , and connected so their magnetic fields oppose each other. The radial component H_r of the magnetic field at a point (r, z) , is given by

$$H_r = \frac{I}{2} \left\{ \frac{h+z}{r \sqrt{(a+r)^2 + (h+z)^2}} \left[-K(k_+^2) + \frac{a^2 + r^2 + (h+z)^2}{(a-r)^2 + (h+z)^2} E(k_+^2) \right] + \frac{h-z}{r \sqrt{(a+r)^2 + (h-z)^2}} \left[-K(k_-^2) + \frac{a^2 + r^2 + (h-z)^2}{(a-r)^2 + (h-z)^2} E(k_-^2) \right] \right\}, \quad (1)$$

where I is the coil current in amperes, H_r is the field in amperes per meter, and $k_{\pm}^2 = 4ar \left[(a+r)^2 + (h \pm z)^2 \right]^{-1}$ are the arguments of the complete elliptic integrals K and E .

b. Field of Two Opposed Semi-Ininitely Long Solenoids. The field of two semi-ininitely long opposing solenoids will be identical to that of two discs uniformly charged with like magnetic charge, $\sigma = nI$, where n is the number of turns per meter, and I is the solenoid current. For a disc at $z = h$ and another at $z = -h$ one finds

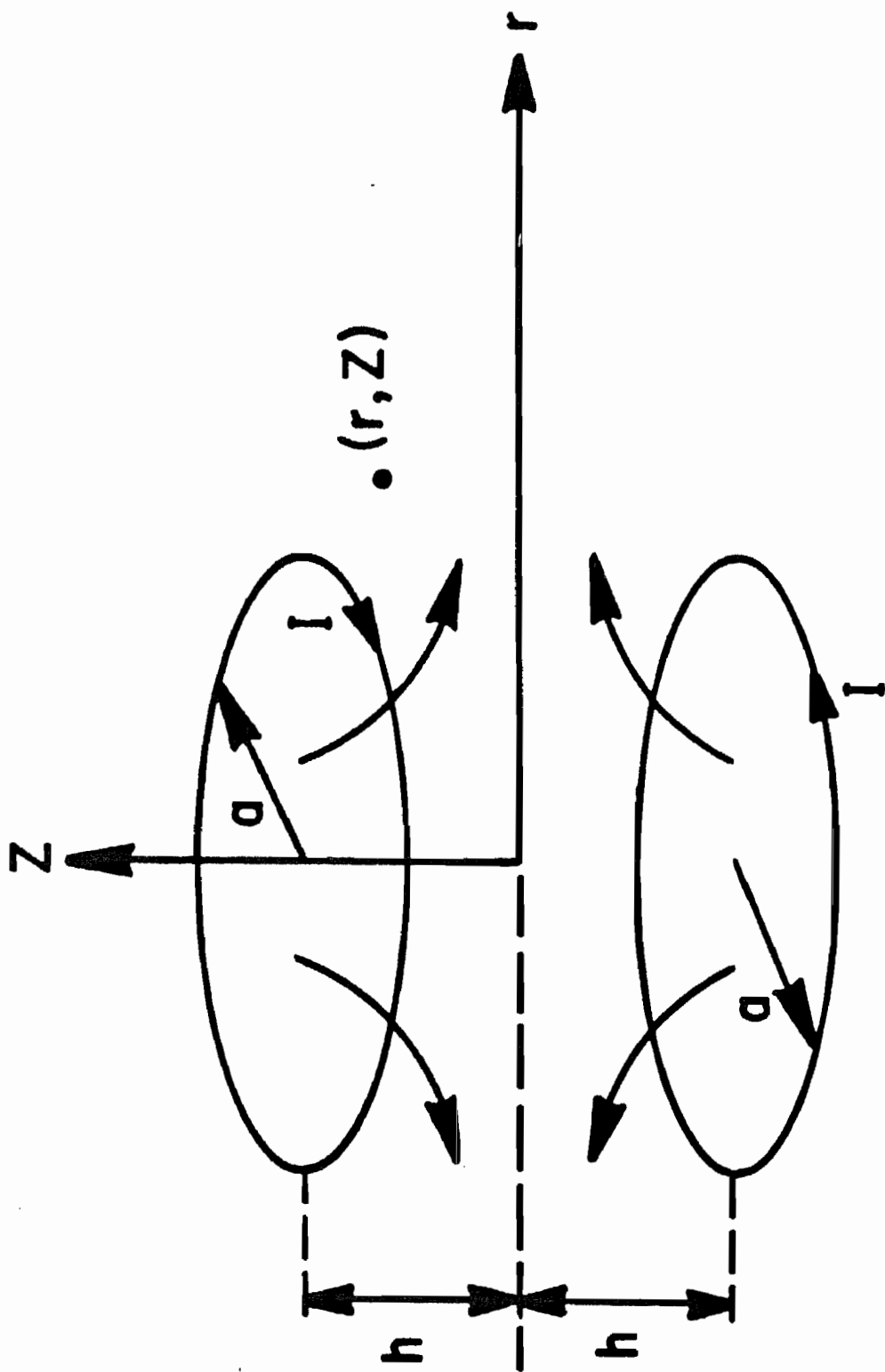


Fig. 1. Magnetic field of opposed current loops.

$$\phi(0,z) = \frac{\sigma}{2} \{ [a^2 + (z+h)^2]^{1/2} - (z+h) + [a^2 + (z-h)^2]^{1/2} - (z-h) \}.$$

Therefore, the potential is given everywhere by the expression (1)

$$\phi(r,z) = \frac{1}{\pi} \int_0^\pi V(z + ir \cos \theta) d\theta,$$

where

$$V(x) = \phi(0,x) \text{ and } i = \sqrt{-1}.$$

Consequently,

$$\begin{aligned} H_r &= -\partial\phi/\partial r = -(1/\pi) \int_0^\pi V' i \cos \theta d\theta \\ &= -\frac{\sigma}{4\pi} \int_0^\pi \frac{(z+h+i r \cos \theta) i \cos \theta}{[a^2 + (z+h+i r \cos \theta)^2]^{1/2}} + \frac{(z-h+i r \cos \theta) i \cos \theta}{[a^2 + (z-h+i r \cos \theta)^2]^{1/2}} d\theta. \end{aligned} \quad (2)$$

An alternate expression for this field (valid for $r > a$) in terms of Legendre polynomials is readily derived and gives identical numerical results. Equations (1) and (2), have been evaluated in the following section.

c. Results and Discussion. Figure 2 shows a three-dimensional plot of the radial field H_r as a function of the source separation distance (h/a) and as a function of radial position (h/a). Particular slices through this figure are shown in Fig. 3. The general shape of the H_r vs r curve is similar for the two cases (current loops and solenoids) and is shown in Fig. 3 for the solenoid. Asymptotically, of course, the solenoid-produced field must fall off as r^{-1} , whereas the current loop field falls off as r^{-2} . The peak moves outward from the axis and broadens as the separation h/a increases. Figure 4 shows the linear variation of peak position for the two cases. Figure 5 shows the linear variation of the width ($\Delta r/a$) vs h/a for $\Delta H_r/H_0 = 100$ ppm, where H_0 is the value of the axial field H_z at the center of a single isolated current loop or solenoid. Figure 6 shows the variation of the

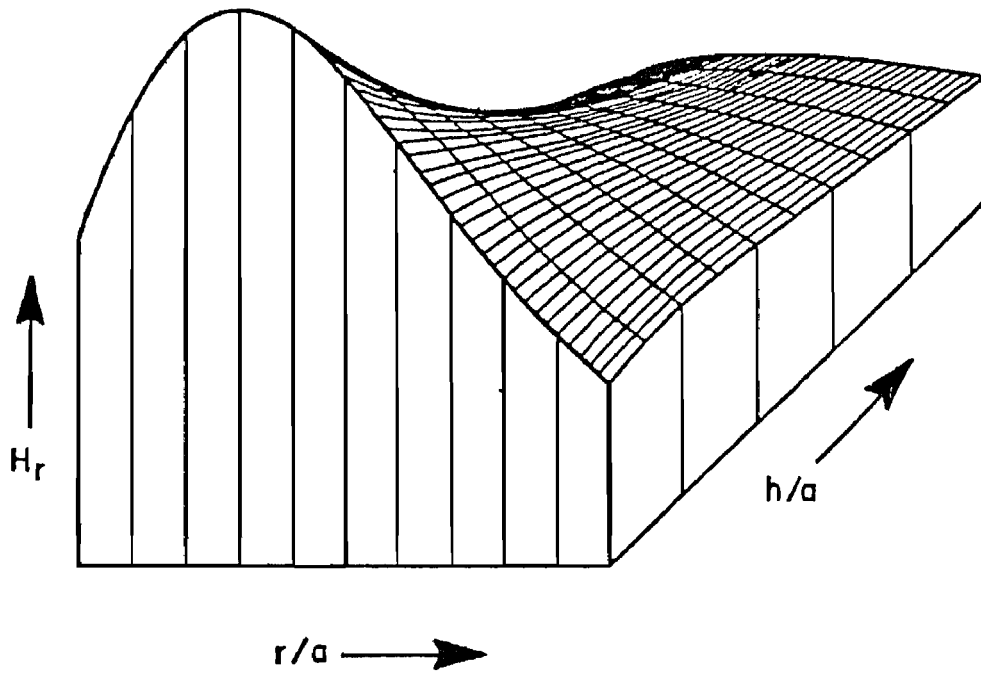


Fig. 2. Three-dimensional plot of H_r vs (h/a) and H_r vs (r/a) .

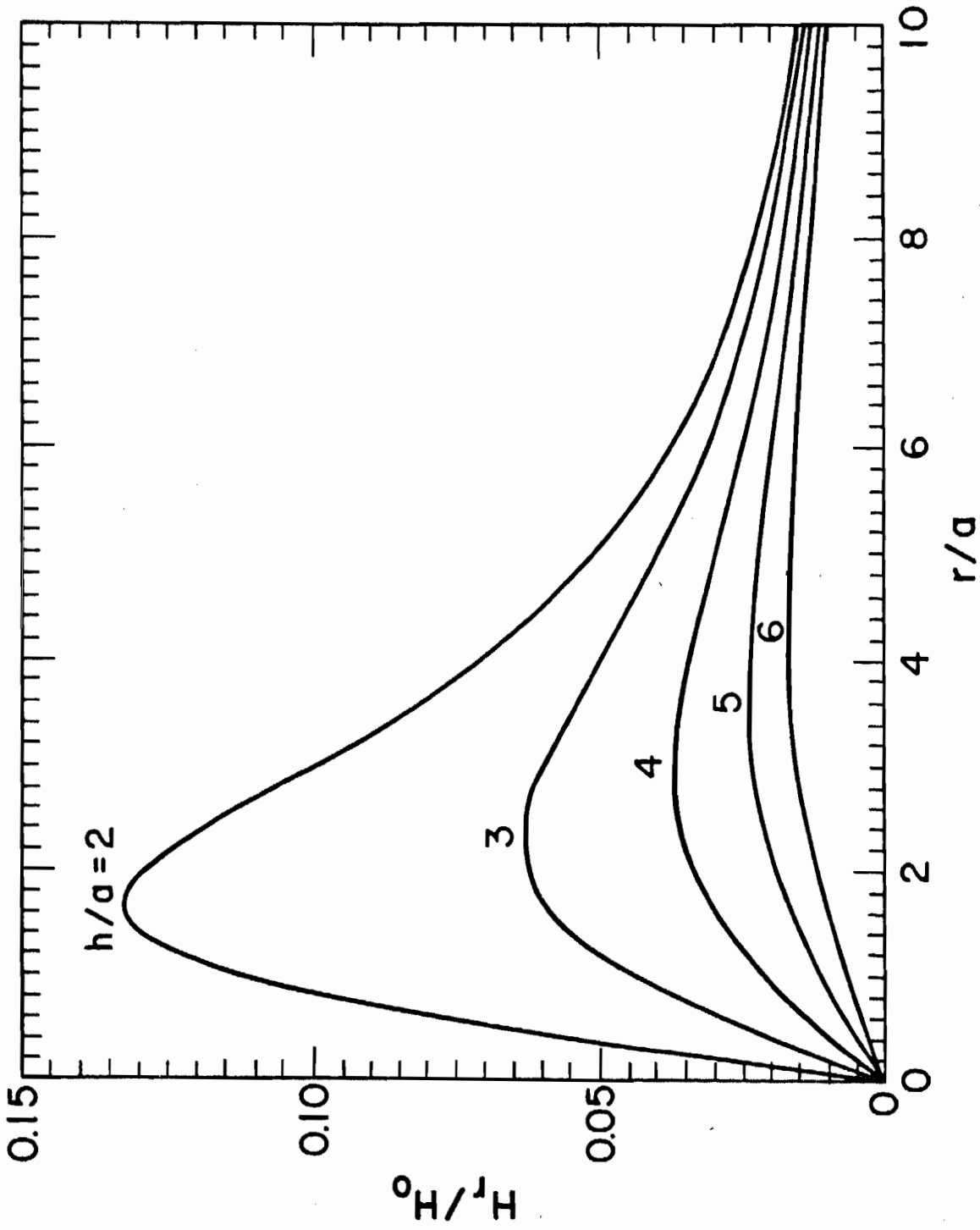


Fig. 3. Variation of the H_r/H_0 vs r for two opposed infinite solenoids of radius a .

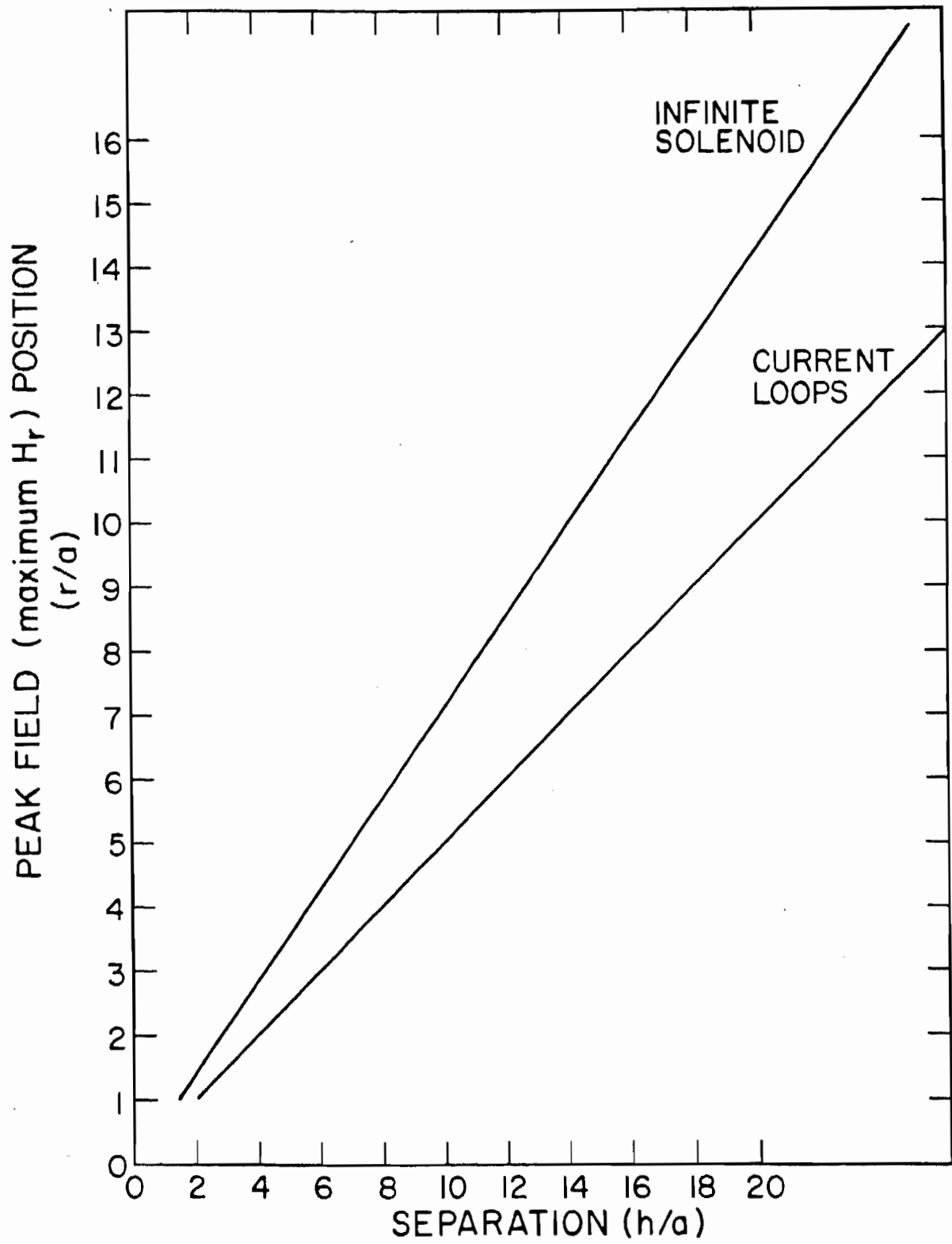


Fig. 4. Variation of peak H_r vs separation of field producing elements (loops or solenoids).

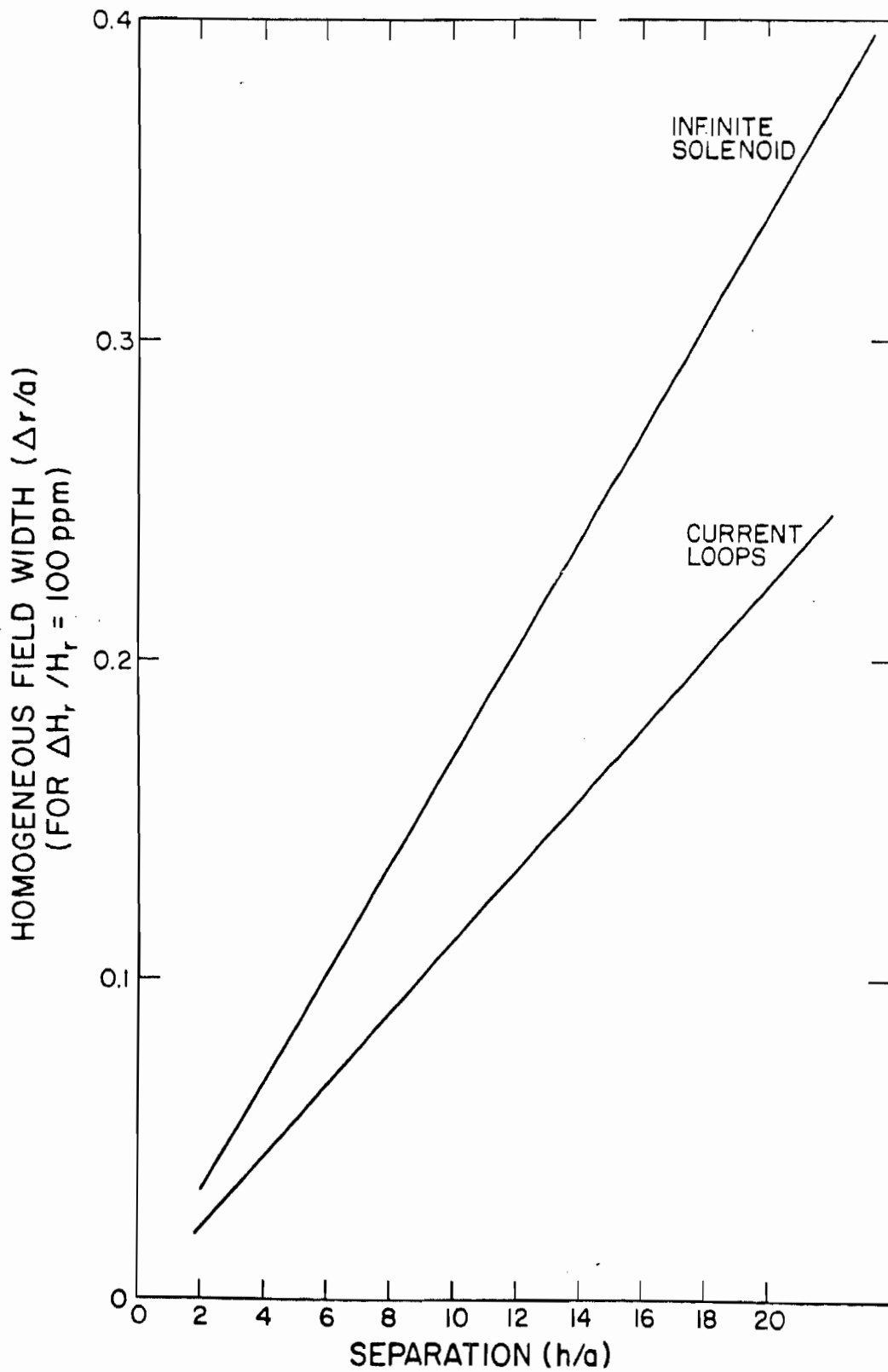


Fig. 5. Variation of homogeneous field width (r/a) in midplane for $H_r/H_r = 100$ ppm.

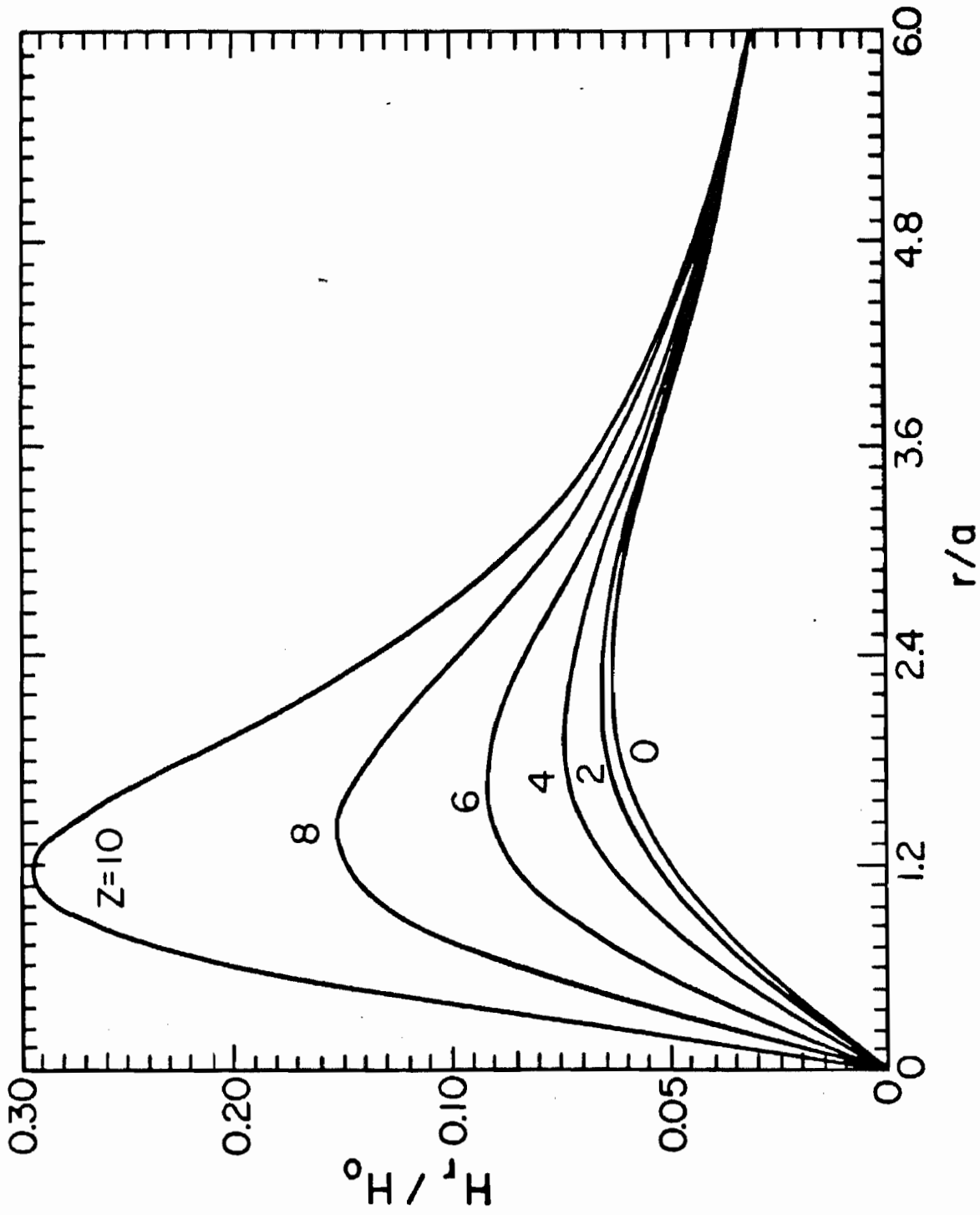


Fig. 6. Variation of (H_r/H_0) with distance from midplane ($z = 0$) for 4-in.- ($a = 5.08$ cm) diam magnets and 1-ft separation ($h/a = 3$).

H_r vs r curve as the distance from the midplane ($z = 0$) is increased. The peak field increases rapidly and moves nearer the axis. Off the mid-plane, of course, the component H_z is no longer zero and increases as z increases. It is apparent from Figs. 5 and 6 that the cross section of the region within which H varies less than any given ΔH will become more flattened as ΔH increases. That is, for very small ΔH , the toroidal cross section will be nearly circular, and for larger ΔH , the height (Δz) will increase more slowly than the width (Δr).

Figure 7 shows the measured radial field in the midplane between two permanent magnets (3 in. square x 6 in. long) and Fig. 8 shows the comparison of peak field strength and peak position vs magnet separation for the measured values and calculated values, where r is measured from the magnet edge.

For a finite length magnet (solenoid), the calculations were made by linearly combining solutions for two sets of discs with opposite charges at the two ends of the magnets.

An example of the result of this type of calculation is shown in Fig. 9, which shows the variation in peak field with magnet length for two 10.16-cm- (4-in.-) diam magnets separated by 39.48 cm, ($h/a = 3$) as the length is varied from 15.24 cm (6 in.) to 60.96 cm (24 in.). It is apparent that the field rapidly approaches that of infinitely long magnets.

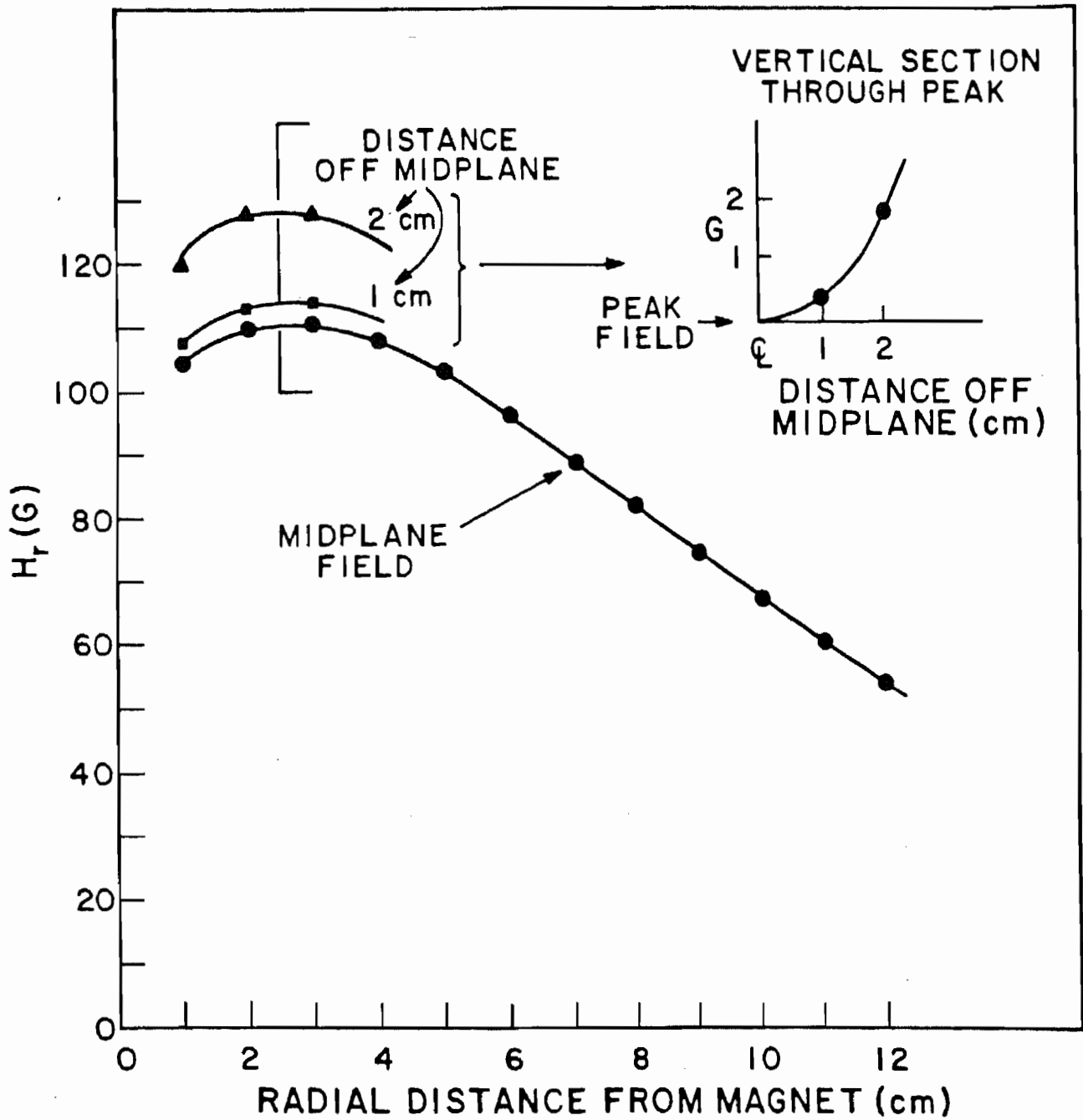


Fig. 7. Measured H_r for two 3-in.-square permanent magnets (6 in. long) as a function of radial distance from magnet edge.

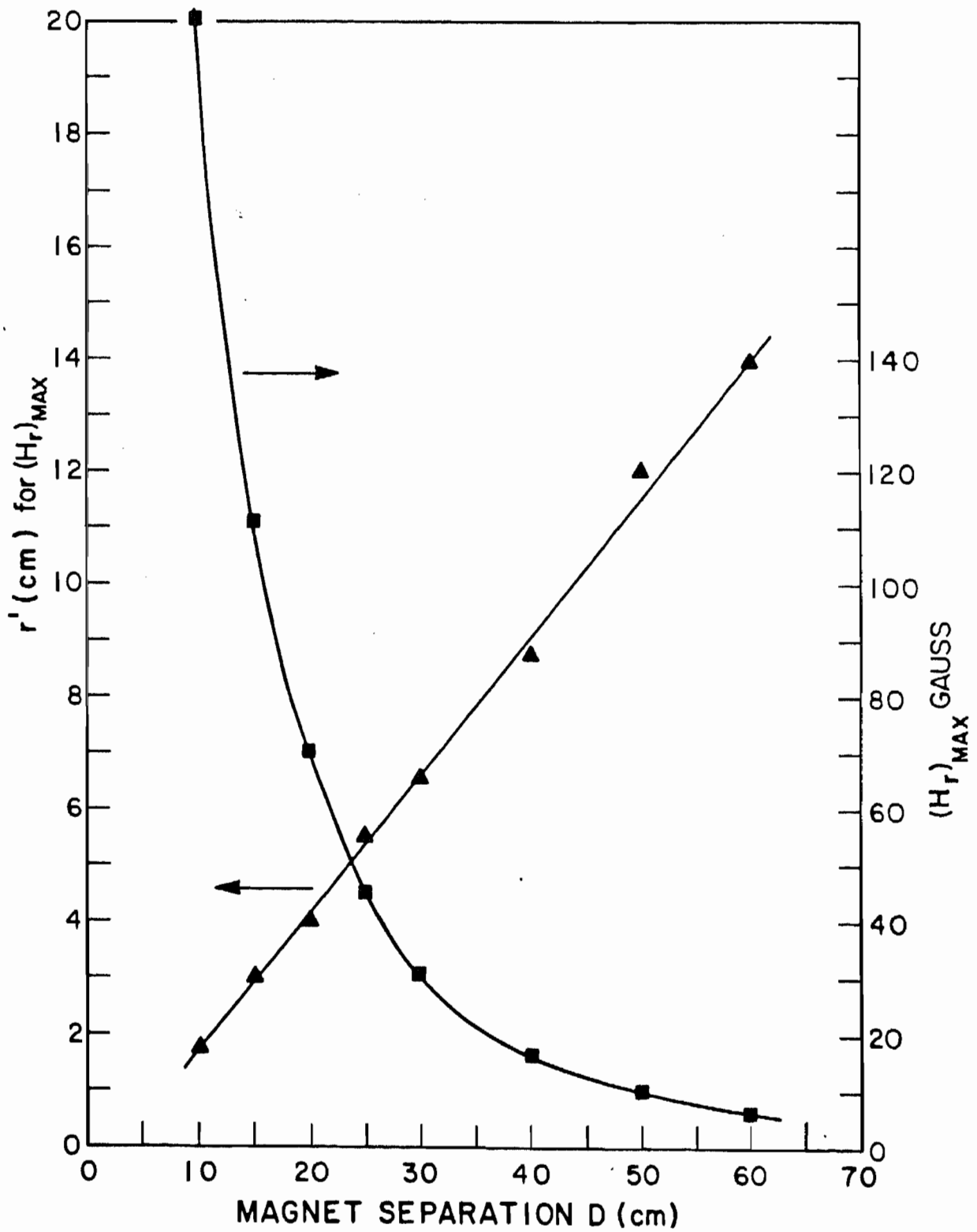


Fig. 8. Measured values of peak positions and field for two 3-in.-square permanent magnets.

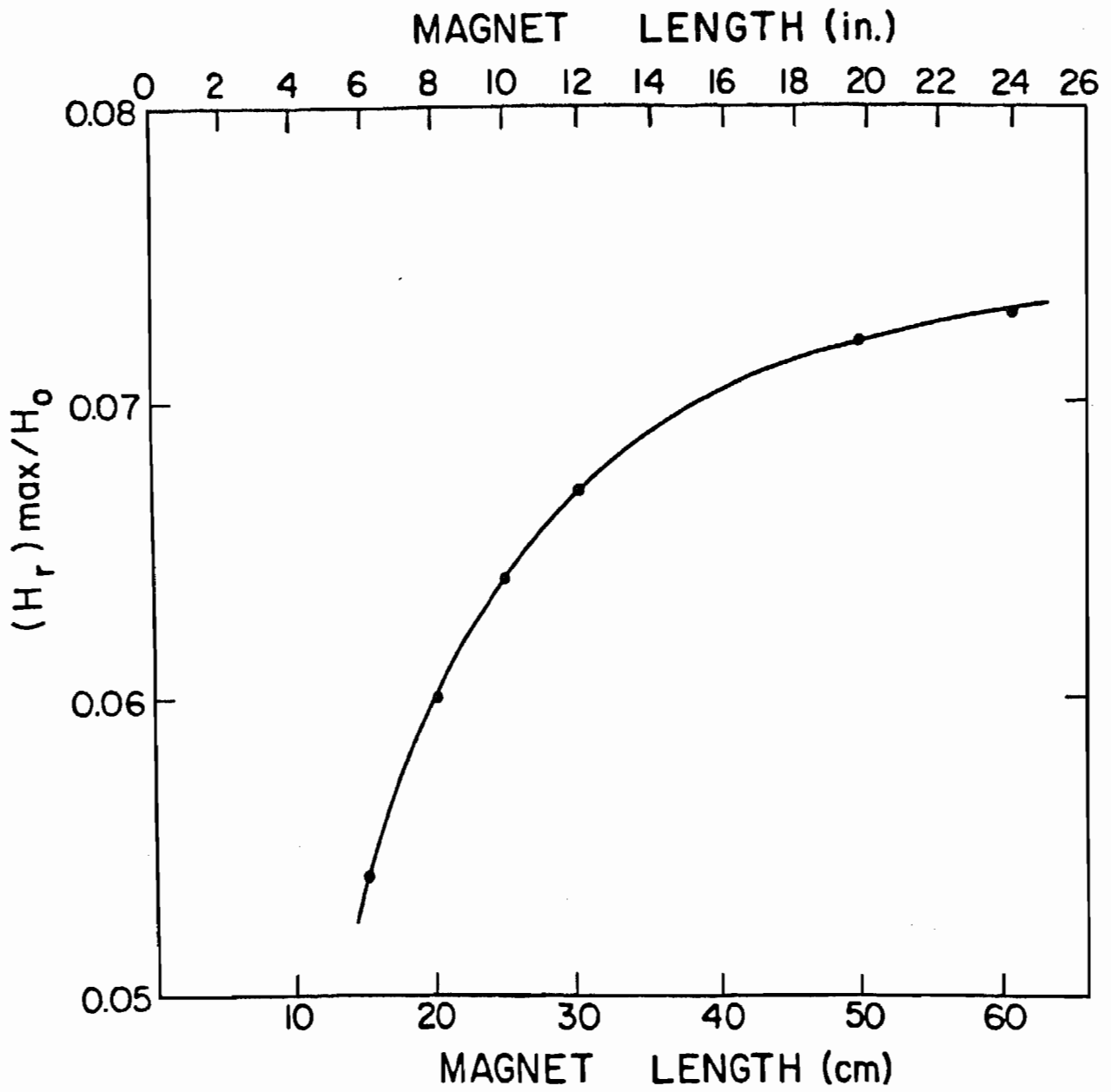


Fig. 9. Calculated variation of peak field for finite length magnets as a function of length. (For $a = 5.08$ cm and $h/a = 3$).

IV. LABORATORY STUDIES: DETECTION OF NUCLEAR MAGNETIC RESONANCE IN A REMOTELY PRODUCED REGION OF HOMOGENEOUS MAGNETIC FIELD

The discovery of a method for remotely producing a toroidal region of homogeneous magnetic field, described in Section I, prompted an analysis of this region (Fig. 10) for practical magnet configurations. The sensitivity of NMR detection from samples located outside the coil has also been investigated (Section V). The results of these studies suggested the possibility of detecting an NMR signal from a sample located in the remote toroidal region.

A. The Experiments

1. Toroidal Region of Homogeneous Magnetic Field. A 4-in. Varian V-4004 electromagnet was modified to provide a toroidal region of homogeneous radial magnetic field centered 14 cm from the magnet axis. For simplicity, we shall refer to it as the "resonance" region. The coils, pole pieces, and pole adjustment mechanisms were removed from the standard iron yoke and mounted in a vertical configuration on an aluminum yoke with brass stabilizing adjustment rods.

Power was supplied by a Varian Model 2200 power supply. This supply was capable of producing a maximum radial field H_r of approximately 120 G in the toroidal region. The upper part of the graph in Fig. 11 shows the variation of H_r vs r , the radial distance from the center of the structure. The width of the region within 100 ppm of the maximum field is about 1 cm. The azimuthal homogeneity was brought to within 0.5 G by adjusting the aluminum yoke and adding magnetic shims to the pole pieces.

Adequate dc stability of the field was provided by the power supply current regulator, and field drift was not observed to be a problem. The field was mapped using a small NMR search coil.

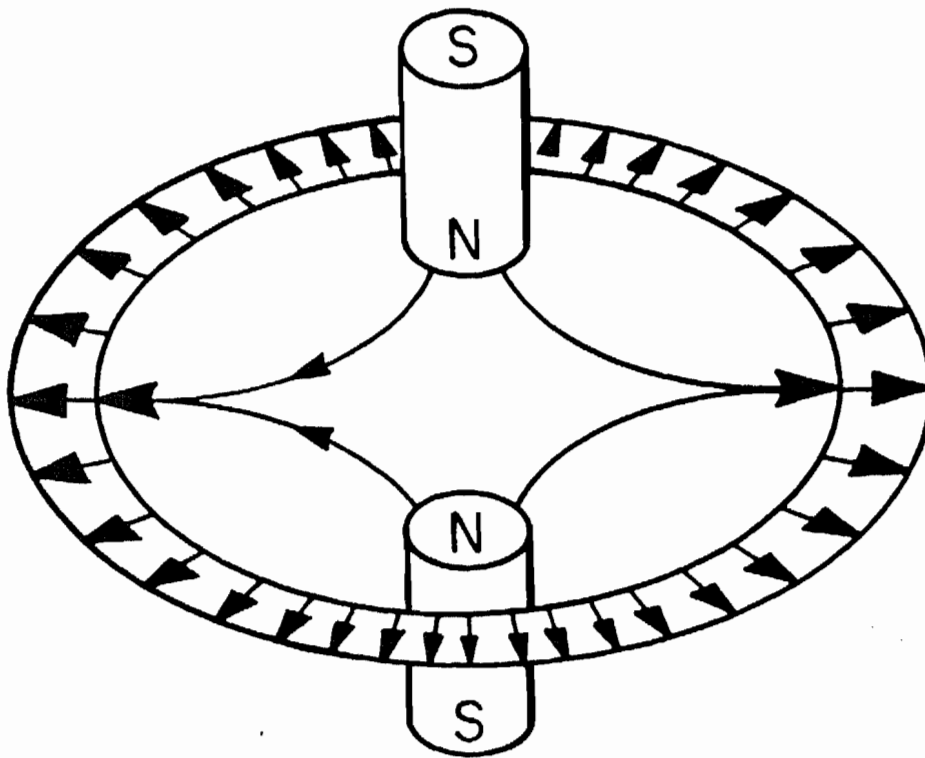


Fig. 10. Magnet configuration for production of toroidal region of homogeneous radial magnetic field.

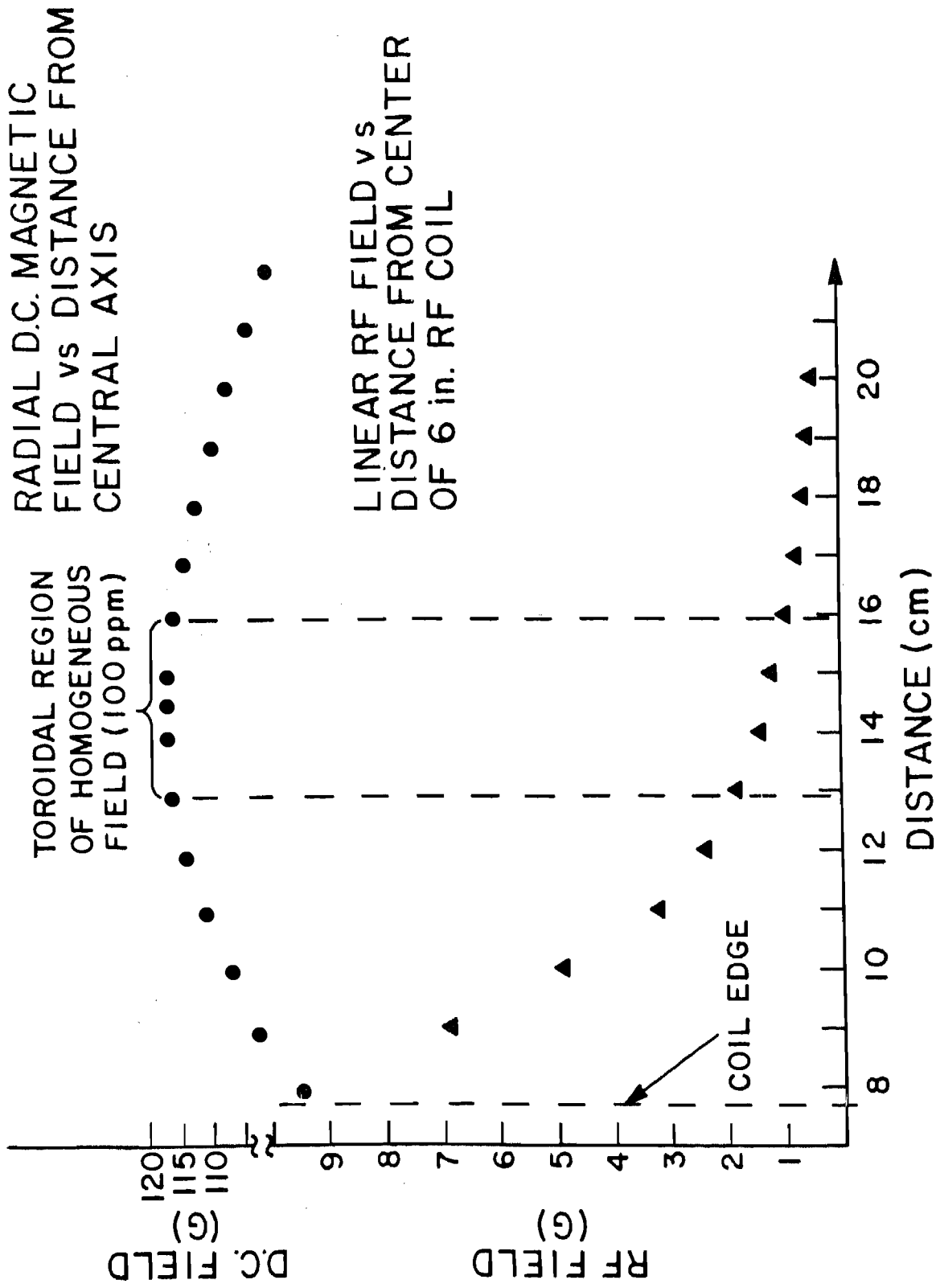


Fig. 11. Upper - D.C. magnetic field plot showing homogeneous region. Lower - rf magnetic field vs distance from coil.

2. NMR Spectrometer. The experimental configuration is shown in Fig. 12. The NMR coil is located coaxially with and midway between the magnet pole faces. This geometry results in symmetric stimulation of the sample by the rf field pulse and equal sensitivity from all portions of the toroidal region. Other arrangements, of course, may be envisioned, which will result in directional sensitivity.

Figure 12 also illustrates the production of a 90° pulse in the sensitive region. In this region, the magnetization is initially aligned along the radial direction and is rotated away from this direction when the rf field is applied.

Following the application of the rf pulse, the magnetization precesses as shown in Fig. 13. The coupling between the precessing magnetization and the NMR coil allows the NMR free induction decay (FID) to be detected. This FID decays with time constant T_2 , the effective spin-spin relaxation time for the sample.

In our present apparatus, the maximum attainable static field in the sensitive region is about 120 G at a radial distance of 14 cm. This limits the maximum proton Larmor frequency to 511 kHz, and the value of 500 kHz was chosen for this experiment.

In order to observe the NMR signal, the spectrometer must be designed to satisfy a number of conditions. The transmitter must be capable of supplying high power radio frequency pulses in order to minimize the rf pulse length and thus the recovery time. The receiver and detection system should be low noise, have a relatively narrow bandpass, and exhibit a short recovery time following the rf pulse. For very low level signals, the capability of signal integration is required.

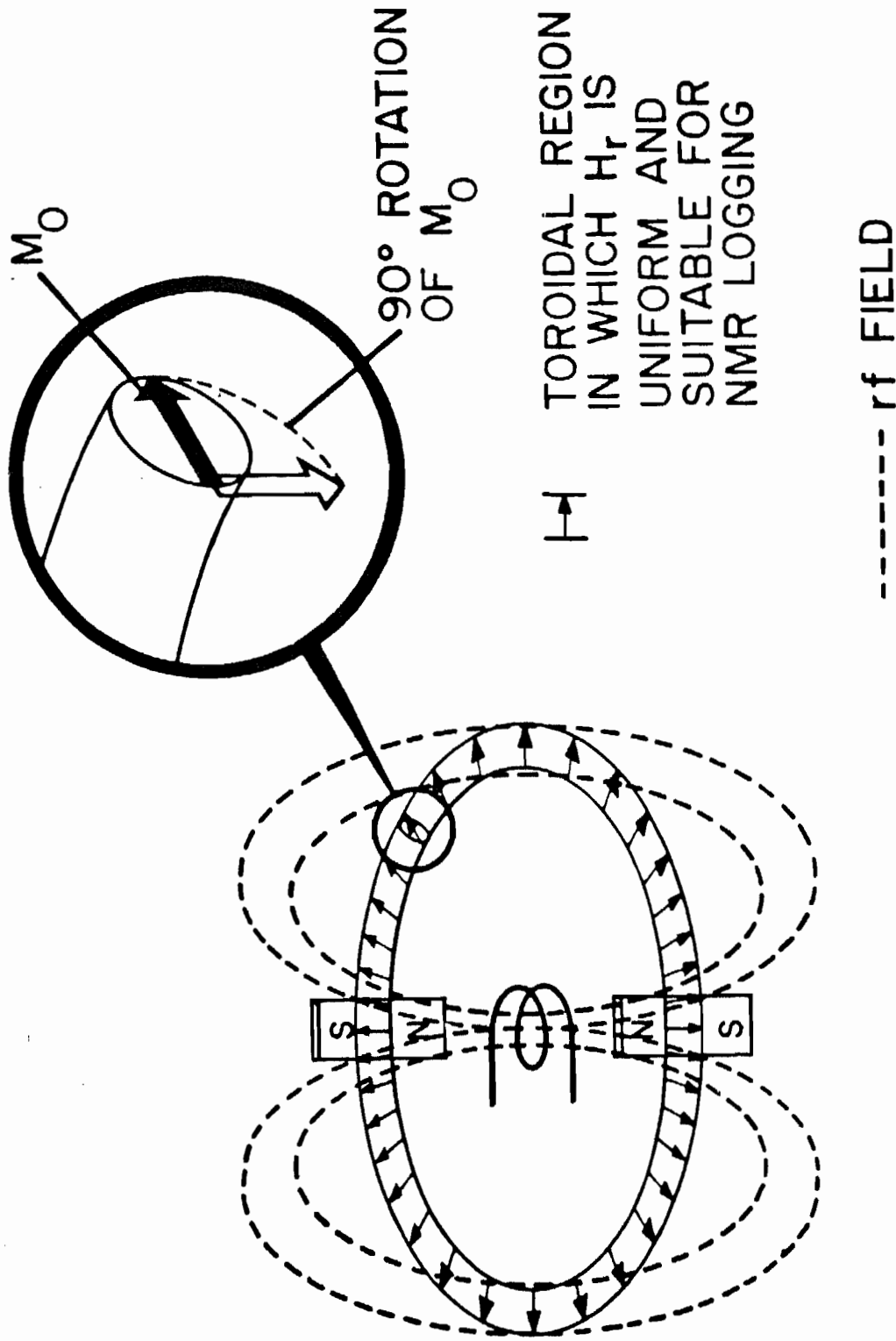


Fig. 12. Production of 90° pulse by rf field at toroidal region of homogeneous magnetic field.

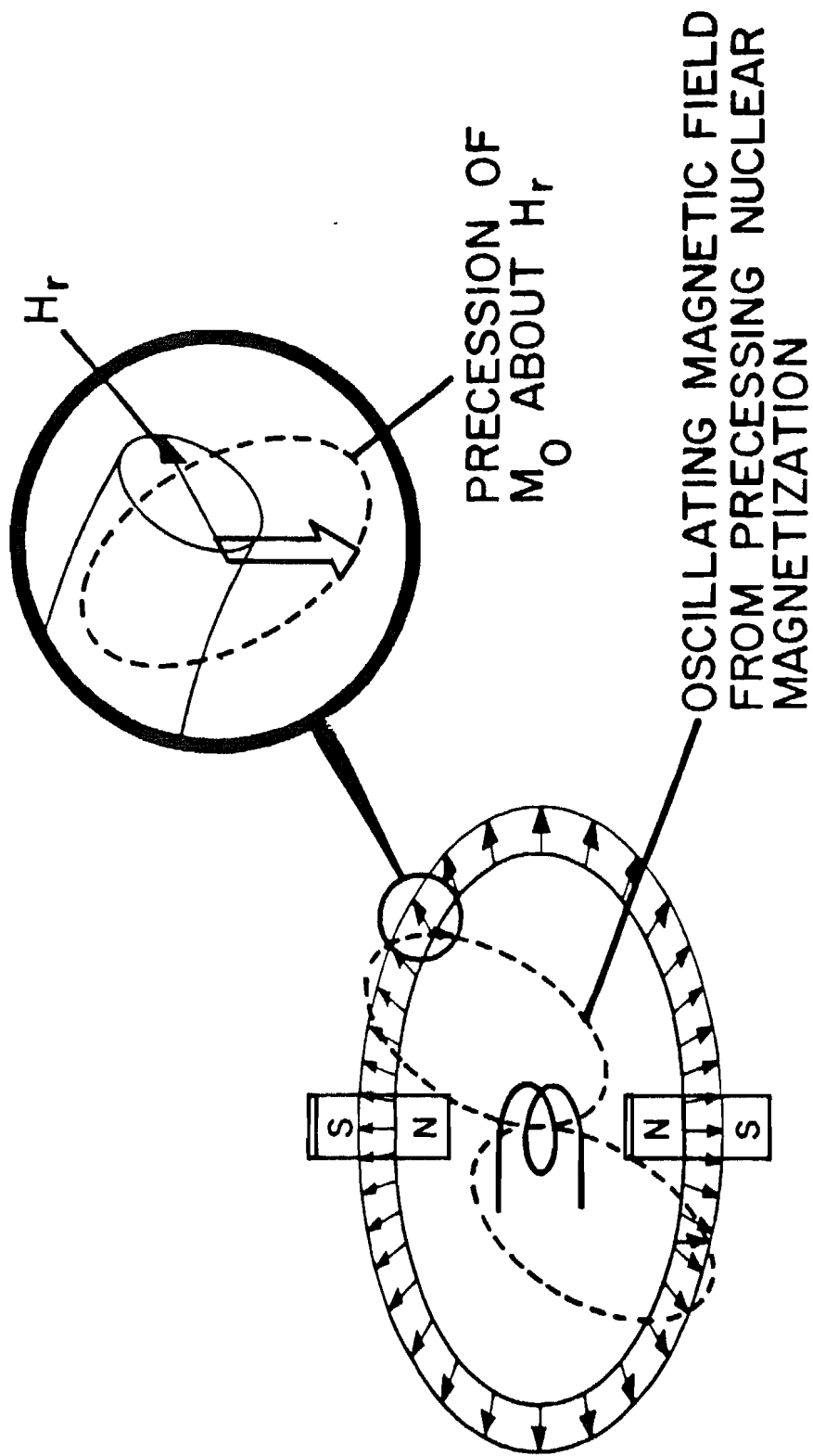


Fig. 13. Induction of voltage in rf coil by precessing nuclear magnetization following 90° rf pulse.

The phase coherent NMR spectrometer for this experiment was of conventional, single coil design. The NMR coil was wound from 10 x 36 Litz wire, 15 cm in diameter and 5 cm high, and was mounted in the midplane between the magnet pole faces. This configuration, shown in Fig. 13, results in equal azimuthal coupling between the sample and the coil. The 15-cm coil diameter was chosen to give a ratio of approximately two between the diameter of the sensitive region and that of the coil. The $50\ \Omega$ output impedance of the transmitter was matched to the sample circuit by connecting the sample coil to operate as an autotransformer. The effective Q of the sample circuit, determined by a measurement of the bandwidth, was 75.

The transmitter was a series of class C amplifiers driven by Hewlett Packard Model 606 signal generator. High peak power is required as the rf field falls off very rapidly with distance outside the sample coil. The peak power of the transmitter was limited to about 20 kW, which was sufficient to produce a 0.94-G rotating H_1 field at the site of the homogeneous region. The lower graph in Fig. 11 shows the linearly polarized rf field strength as a function of radial distance from the center of the sample coil. These data were taken for a set of conditions typical for our experiments.

The sample circuit was damped at the preamplifier input by a gated MOSFET damper. At these low Larmor frequencies, spectrometer recovery times are often quite long due to ringdown of the High-Q sample circuit. Insertion of the active damper allowed the NMR FID to be observed at times less than 200 μ s from the beginning of 30- μ s transmitter pulse.

A low-noise preamplifier with a 20-kHz bandwidth and a gain of 10 was designed using an Optical Electronics Inc. (OEI) Model 9913. The preamplifier was followed by a wide bandwidth amplifier and a phase detector of conventional

design. A Princeton Applied Research Model 4202 signal averager was used to extract the signals.

B. Results

Signals were detected from the sensitive region of remotely produced field for two distant sample geometries. First, a small toroidal sample was fashioned using a 1.0-cm-i.d. Pyrex tube filled with glycerol. This sample was located in the sensitive region sketched in Fig. 14. Later a larger 2.5-cm-i.d. glycerol-filled tygon tube was used.

The proton signal obtained from this sample is shown in Fig. 15. The observed pattern is a beat between the induced-decaying NMR signal and a reference rf signal. In order to enhance the signal-to-noise (S/N) ratio, these data were taken with a 24-cm-diam rf coil and the signal was averaged over 400 FID scans. Proof that the signal came from the sensitive region is found in the fact that the placement of this sample is critical, and that no signal could be observed when the sample was moved off center by as little as one sample diameter (2.5 cm).

Next, a glycerol sample was constructed that filled a large volume surrounding and including the sensitive region. This sample geometry, which is analogous to the situation in potential applications, is shown in Fig. 16. The proton NMR signal, obtained with the 15-cm rf coil, is shown in Fig. 17. This signal is the result of 12,000 FID scans and indicates a S/N ratio of approximately 1 to 20.

To further demonstrate that the detected signals came from the same toroidal region of remotely produced homogeneous field, the FID T_2 decay times were compared for the signals from these two geometries. In the first case, that of sample only in the sensitive region, the observed $T_2 = 350 \pm 35 \mu\text{s}$. The observed value for the case where a large region is filled with

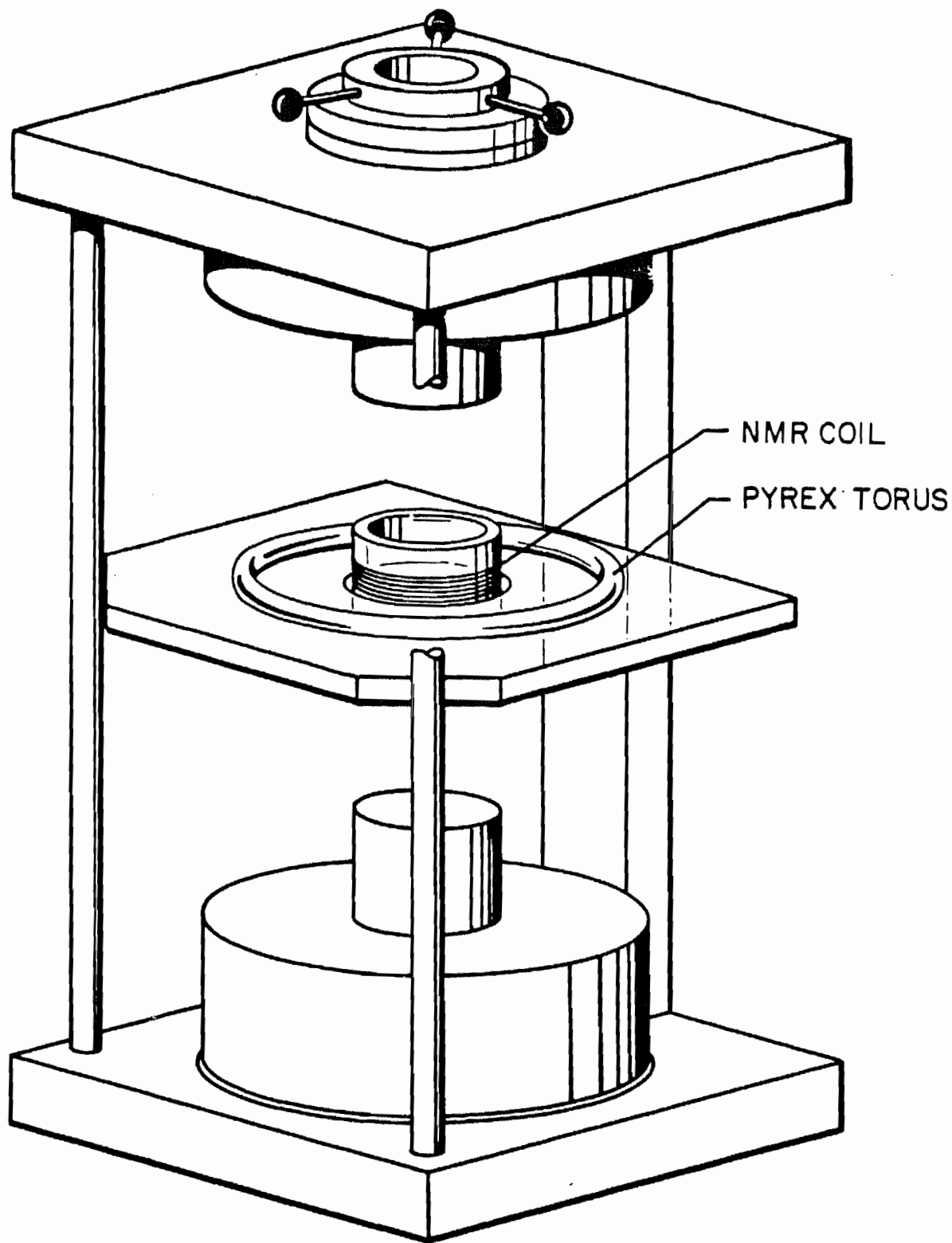


Fig. 14. Glycerol-filled pyrex annulus mounted at $r = 14$ cm in midplane of magnet.

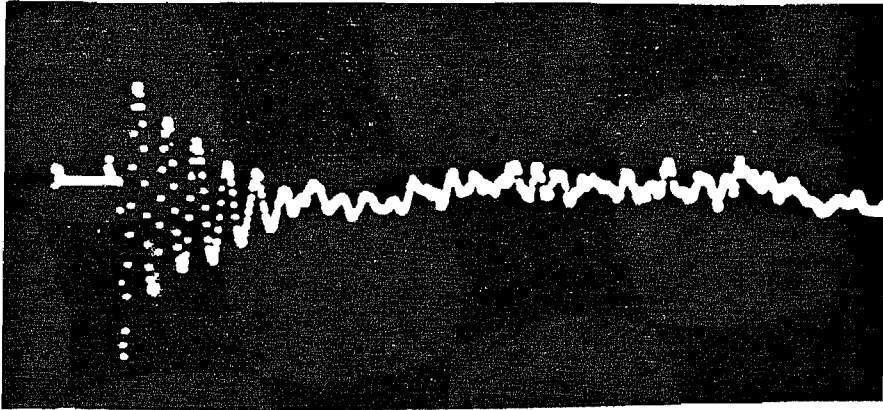


Fig. 15. Proton NMR signal from glycerol-filled tygon torus at $r = 14$ cm.

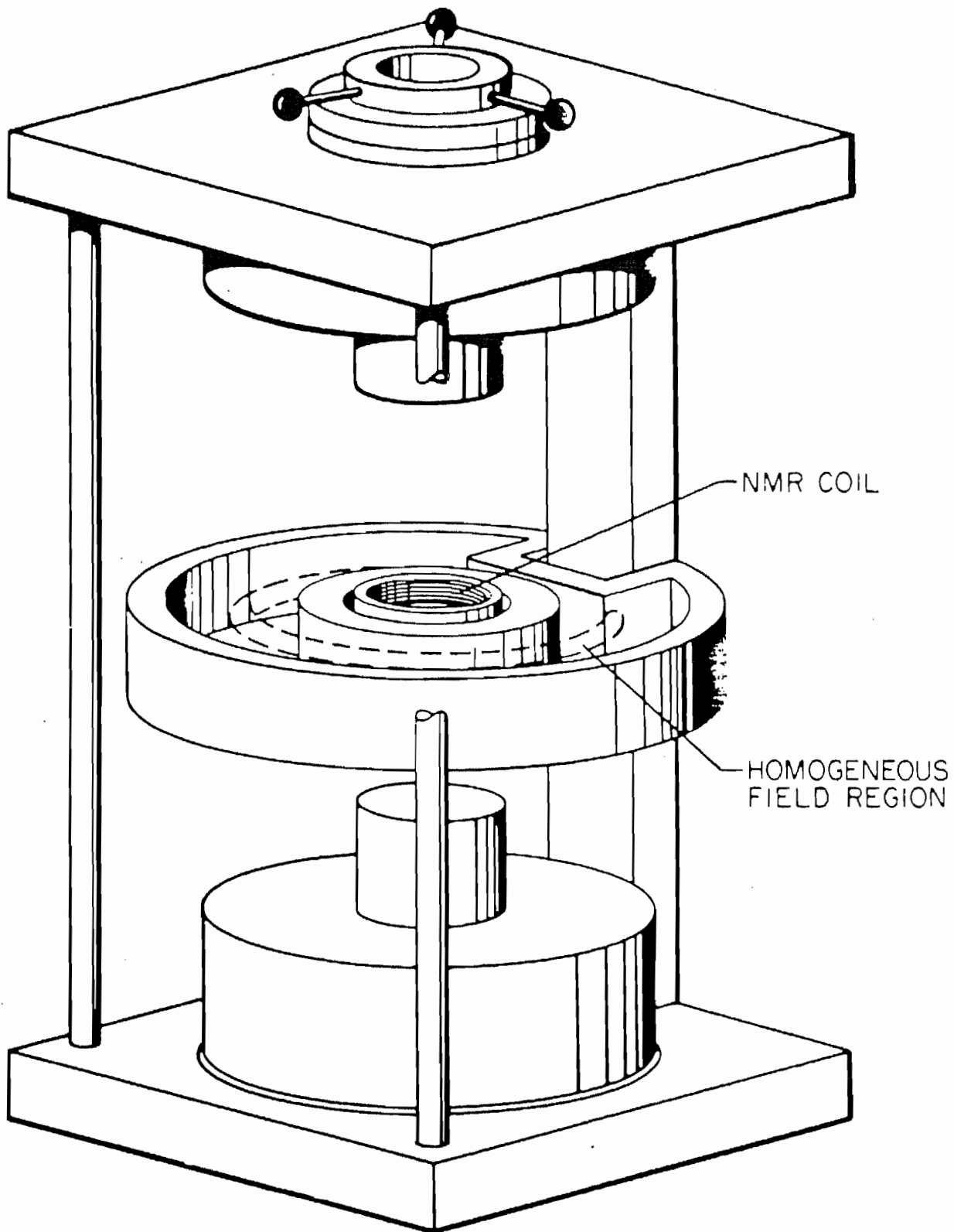


Fig. 16. Glycerol-filled styrofoam tub surrounding rf coil in magnet mid-plane.

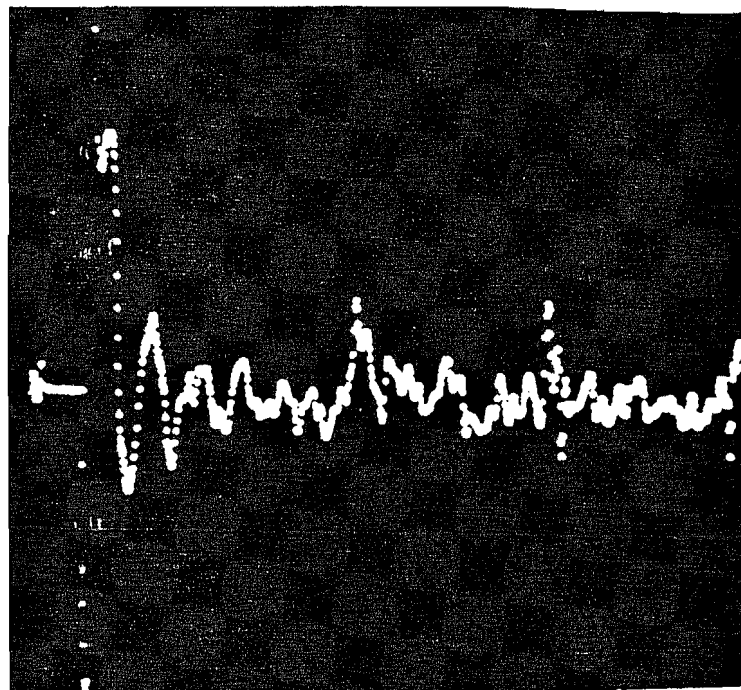


Fig. 17. Proton NMR signal from the homogeneous toroidal region in a glycerol-filled tub at $r = 14$ cm.

sample was $T_2 = 350 \pm 100 \mu s$, in which the larger uncertainty resulted from the use of a smaller rf coil more remote from the sensitive region. The similarity of these decay times is further evidence that the signals actually arise from the same region of magnetic field.

A preliminary estimate of the voltage expected to be induced in the coil can be obtained from the expression

$$V = NQA_C B \omega_0 t,$$

where N = number of turns on NMR coil,

Q = quality factor of NMR coil,

A_C = area of NMR coil,

B = field at center of NMR coil due to sample magnetization, and

ω_0 = resonant frequency.

For our experimental parameters, the expression gives $V \approx 10 \mu V$. Using the observed output noise level of ~ 200 mV, this predicts and measures system gain of ~ 3000 S/N of $\sim 1/20$ in reasonable agreement with the observed S/N.

A series of measurements were made with the glycerol-filled tygon torus at $R = 14$ cm using coil from 9 in. to 5 in. diameter. These data suggest that the signal varies as $(R/a)^{-5}$. For the normal case where a is constant and R varies, the signal should vary as $(R/a)^{-2}$ because the width ΔR of the homogeneous region varies directly as R and the sample volume $V \propto R(\Delta R)^2 \propto R^3$; i.e., $(S/N) \propto (1/R)^2$, all other factors being held constant.

A detailed study of the expected signal amplitudes and S/N ratios is quite complex and is currently under study. However, it is clear that a substantial improvement in the S/N ratio may be obtained by improving both the spectrometer recovery time and the homogeneity of the toroidal region. As an example of the latter, a T_2 of $2 \mu s$ or longer was routinely observed at particular locations in the toroidal region using a sample of approximately

1 cm³ and our NMR field mapping apparatus. A more flexible magnetic structure, now under development, will allow much better homogeneities to be obtained.

V. SENSITIVITY OF NMR DETECTION FOR EXTERNAL SAMPLES

Although there are a variety of geophysical applications that require the sample to be in a position remote from the spectrometer, very little on the experimental particulars of this configuration has been published. Here we present the results of sensitivity measurements for cylindrically symmetric samples located outside the sample coil. The results are analyzed in terms of a simple model that may be useful in extrapolating to cases of greater geometrical complexity.

A. The Experiments

In experiments where the sample must be located outside the sample coil, away from the region of the spectrometer, often a relatively small value of H_0 , the DC polarizing field, will be available. For these experiments we chose a frequency of 500 kHz, corresponding to an H_0 field of 117.5 G. This field was produced by a 10-in.-diam Helmholtz pair powered by a Magnion HSR-1365B power supply.

The transmitter for the spectrometer was an Arenburg Model PC-650C pulsed oscillator. The receiver was designed using an OEI Model 9913 low noise pre-amplifier and OEI Model 9917 Op Amp in the gain-controlled receiver. Linear envelope detection was used and the receiver system had a gain of about 3000. The bandwidth was approximately 10 kHz, and the spectrometer had a recovery time of 200 to 300 μ s following the pulse. For these measurements, the pulse length was adjusted to give a maximum FID signal.

The sample coil was 2.5 cm in diameter by 1.7 cm in length. The sample circuit was parallel tuned and operated as an autotransformer in order to match the output impedance of the transmitter. Crossed diodes, in both the transmitter output and receiver input, operated as Q-switching devices to reduce

the recovery time while maintaining a high S/N ratio. The Q of the sample circuit with the transmitter off, i.e., during observation, was measured to be about 50, while the Q during a pulse was estimated to be about 5.

The samples were annular in shape and were formed by filling concentric, flat-bottom pyrex cups with glycerol. The sample geometry is illustrated in Fig. 18. From a set of six cups, a series of eight annular samples of various inside and outside diameters was formed. Inside diameters ranged from 1.1 to 2.3 sample coil diameters, and outside diameters ranged from 1.3 to 2.5 sample coil diameters. The radial dimensions of the annular samples are listed in Table 1. The samples were approximately 20 per cent longer than the sample coil.

A conventional cylindrical sample of glycerol in a 1.5-cm o.d. test tube served as a reference. This sample also extended beyond the sample coil, and careful measurements of the response of the spectrometer to small samples located above and below the coil indicated that a systematic correction of 10 per cent to the relative sensitivity was required. The magnitude of the signal from the reference sample was compared directly to the measurements made on the annular samples. A PAR model CW-1 Boxcar Detector, combined with an X-Y recorder, was used to extract and display the NMR FID. As the inhomogeneity of the dc field over the sample volume was different for each sample configuration, differing FID decay times were observed for each data set. In order to compensate for this effect, the magnitude of the signal was extrapolated to the beginning of the pulse, i.e., through the recovery time. This extrapolation introduced uncertainty of about 10 per cent into the measurements.

B. Results and Discussion

Measurements of the FID signal amplitudes obtained for both the annular and reference samples yielded the results shown in Fig. 19. The quantity g is

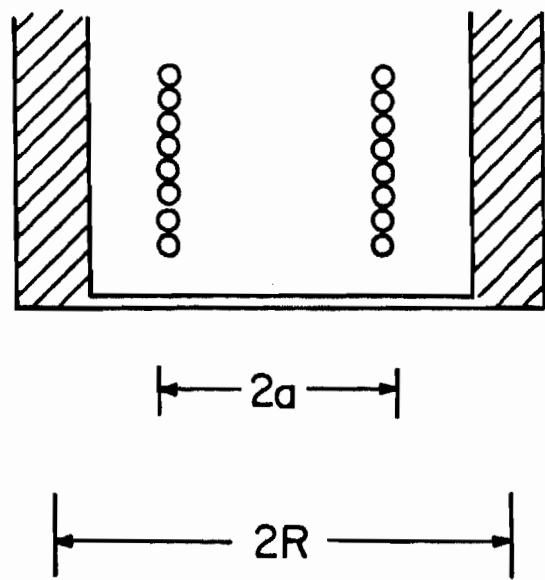
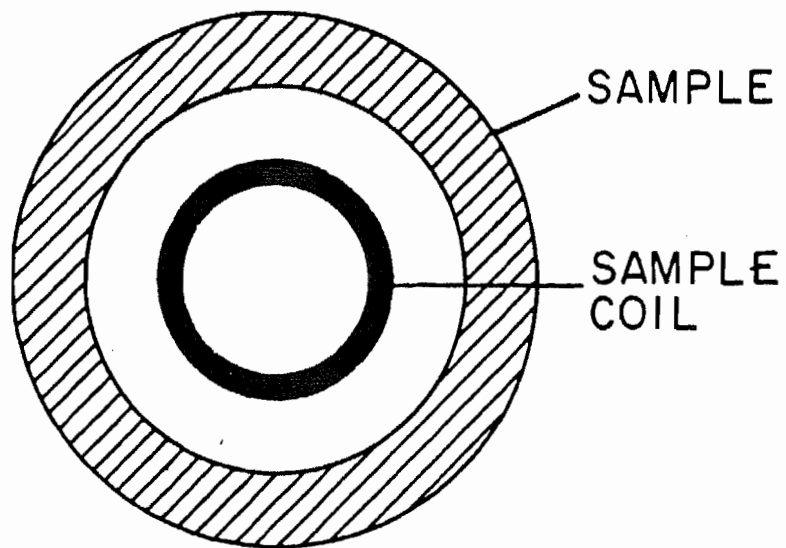


Fig. 18. Geometry of the cylindrically symmetric external samples.

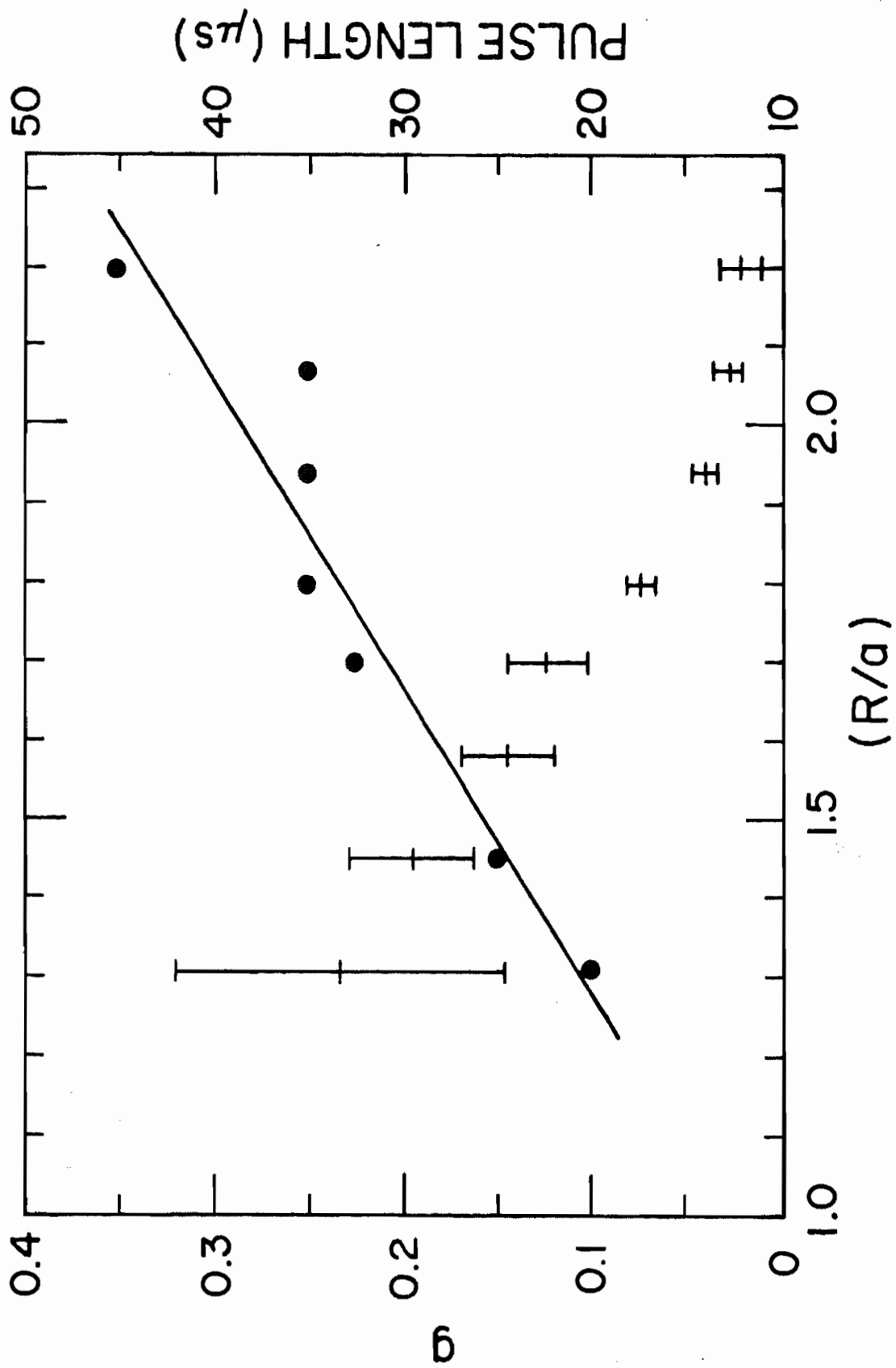


Fig. 19. Plot of the relative signal per unit volume g (+) and the rf pulse length X vs (R/a) .

TABLE I
RADIAL DIMENSIONS OF THE ANNULAR SAMPLES

<u>Sample No.</u>	<u>Inner Diameter (mm)</u>	<u>Outer Diameter (mm)</u>	<u>R/a</u>	<u>(a/R)³</u>
1	31.85	33.85	1.31	.445
2	31.85	40.55	1.45	.328
3	31.85	47.10	1.58	.254
4	37.75	47.10	1.70	.204
5	37.75	52.00	1.80	.172
6	44.75	52.00	1.94	.137
7	44.75	58.60	2.07	.113
8	51.25	58.60	2.20	.094

defined as the signal amplitude E_a per unit volume V_a for the annular samples divided by the signal amplitude E_r per unit volume V_r for the reference sample. That is,

$$g \equiv (E_a/V_a)/(E_r/V_r), \quad (3)$$

and is referred to as the relative signal per unit volume. The quantity along the horizontal axis is the ratio of R , the average radius of the annular sample, to a , the radius of the sample coil. In these calculations, R was taken to be the simple average of the inside and outside diameters of the annulus rather than a more complex average based upon proton density. Each data point represents the average of several measurements, and the uncertainties represent one standard deviation.

For each annulus, the rf pulse length was adjusted for maximum FID amplitude. These optimum pulse lengths are also plotted vs (R/a) on Fig. 19.

Over the limited range studied, the data suggest the linear relationship indicated by the fitted straight line.

An estimate of the relative sensitivity per unit volume g can be obtained readily if a number of restrictive assumptions are made. For an N -turn sample coil of radius a and quality factor Q in a resonant circuit, Faraday's Law becomes $E = -NA(d\phi/dt)$ with flux $\phi = \vec{B} \cdot \vec{A}$. For the annular samples, only a fraction of the total flux is linked, and the appropriate area \vec{A} is the cross-sectional area of the sample coil, $A_C = \pi a^2$. For the reference sample, placed within the sample coil, all the flux due to the precessing magnetization is linked. Therefore, A becomes the cross-sectional area of the sample itself, $A_r = \pi d^2$, where d is the radius of the reference sample.

The field is $\vec{B} = B_\rho \cos \omega_0 t$, with ω_0 the Larmor frequency of the precessing magnetization. The peak value is $B_\rho = 4\pi M$ for the reference sample, where the magnetization is $M = \mu_\rho n f$. In this expression μ_ρ is the proton magnetic moment, n is the number density of protons in the sample, and f is the Boltzmann factor or the fraction of protons contributing to the net magnetization.

For the annular samples, $B_\rho = \mu_a/R^3$, where the net nuclear moment of a sample with volume V_a is given by $\mu_a = MR_a$. There are a number of assumptions implicit in the use of this simple relationship. First, it is assumed that all nuclei in the annular sample are located a distance R from the center of the sample coil. Several of our annular samples were relatively thick and it is not clear that this assumption is justified. A more serious reservation, however, arises from the fact that this expression assumes essentially a two-dimensional geometry and $R \gg a$. In our case, the radius of the sample coil is smaller than its length, which is certainly not two-dimensional. In addition, most of our measurements were taken in the region $R \leq 2a$ so

that the field from the precessing nuclei varies significantly over the region of the sample coil. From these considerations it would, in fact, be surprising to observe a strict $(1/R^3)$ dependence of B_ρ .

Combining the expressions for the annular geometry gives the voltage induced in the sample coil

$$\begin{aligned} E_a &= NQA_{c\omega_0} B_\rho \sin \omega_0 t \\ &= NQA_{c\omega_0} (M_z/R^3) \sin \omega_0 t, \end{aligned}$$

or

$$(E_a/V_a) = (NQA_{c\omega_0} M/R^3) \sin \omega_0 t. \quad (4)$$

Similar manipulation of the expressions for the cylindrical reference sample results in

$$E_r = NQA_{r\omega_0} (4\pi M) \sin \omega_0 t$$

and

$$(E_r/V_r) = (4\pi NQ\omega_0 M/l) \sin \omega_0 t, \quad (5)$$

where l is the length of the reference sample and $V_r = A_r l$.

Combining Eqs. (4), (5), and (6) gives the relative signal per unit volume

$$g = a^2 l / 4R^3, \quad (6)$$

which is a relatively simple expression involving only fundamental geometric parameters. When g of Eq. (6) is plotted vs $(a/R)^3$, it results in a straight line with slope $(1/4a)$. For our experimental configuration, this is the solid line shown in Fig. 20, a plot of g vs $(a/R)^3$.

Given the assumptions implicit in Equation (6), we find it surprising that the experimental situation is represented as closely as it is. Overall, the sensitivity data replotted in Fig. 20 suggest an asymptotic approach to a $(1/R^3)$ dependence for $R \gg a$. For $R \sim a$, the measured sensitivity is somewhat greater than predicted and appears to fall off faster than $(1/R^3)$.

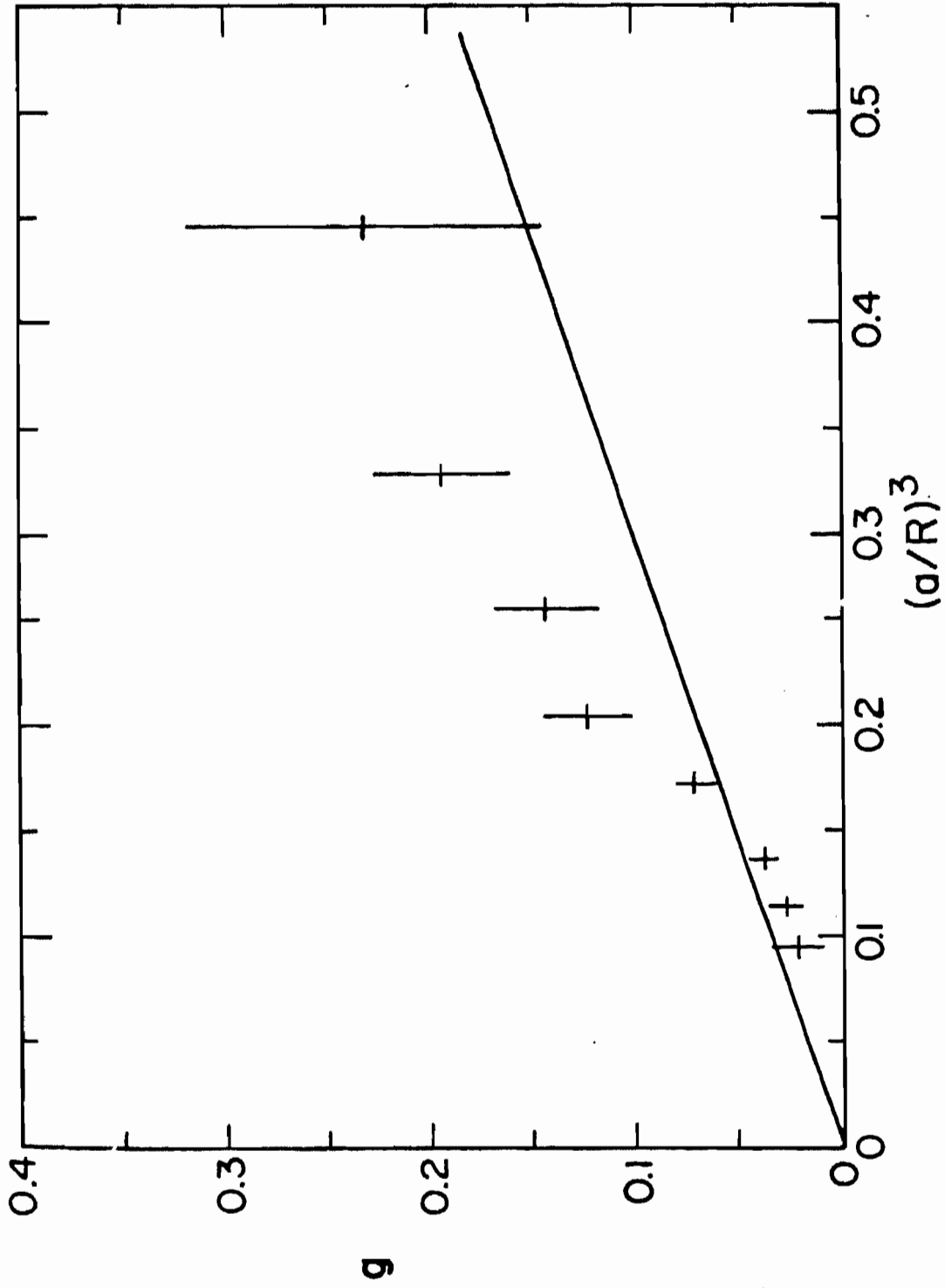


Fig. 20. Plot of the relative signal per unit volume as a function of $(a/R)^3$. The solid line is the prediction of Eq. (6).

In the region R 2a, the sensitivity is somewhat less than predicted. We attribute this to the fact that the field of the rf pulse from the sample coil, used to tip the nuclei from their equilibrium alignment, is very inhomogeneous over the annular sample volume. Therefore, even though the rf pulse length was adjusted for maximum FID amplitude, not all regions of the annular samples experienced an optimum-length 90° pulse. This effect reduced the apparent sensitivity, and may be responsible for the linear relationship observed between the rf pulse length and (R/a) .

VI. PROTOTYPE DOWNHOLE TOOL DEVELOPMENT

A cross section of a particular tool design under consideration is shown in Fig. 21. Figure 21 also shows a plot of the magnetic field strength within the homogeneous resonance region and the NMR resonant frequency as a function of radial distance from the borehole centerline and depth into the formation. The solid line shows the result of computer calculations and the dotted line shows measurements on a normal wire mockup of the superconducting magnets scaled to the fields in the superconducting case.

The following procedure then was used in estimating the NMR S/N ratio for signals received from different distances into the formation surrounding the wellbore. Because the particular tool design under consideration uses an 8-in.-diam rf coil, experimental data from the 8-in. coil in a series of experiments with the laboratory electromagnet were used to estimate the S/N to be expected from a tool using superconducting magnets. This series of experiments was conducted using a fixed toroid and varying the size of the rf coil. The results suggest that S/N varies as $(R/a)^{-5}$. For the normal case where a (radius of magnet) is constant and R (radius of torus) varies, S/N should vary as $(R/a)^{-2}$ because the width R of the resonance region varies directly with R and the resonance volume $V \propto R(\Delta R)^2 \propto R^3$. In other words, $(S/N) \propto (1/R)^2$, with all other factors being constant.

It is also necessary to include the dependence of S/N on the rf frequency. It is known that NMR S/N is approximately proportional to the square of the frequency. The 8-in. coil electromagnet data (S/N = 4.5:1 in 18 s) then were taken at a frequency of 0.5 MHz and a toroidal radius of 14 cm (5.51 in.). Therefore, the S/N to be expected at a radius R and frequency f can be estimated as

$$(S/N) = 4.5 \times (5.51/R)^2 \times (f/0.5)^2.$$

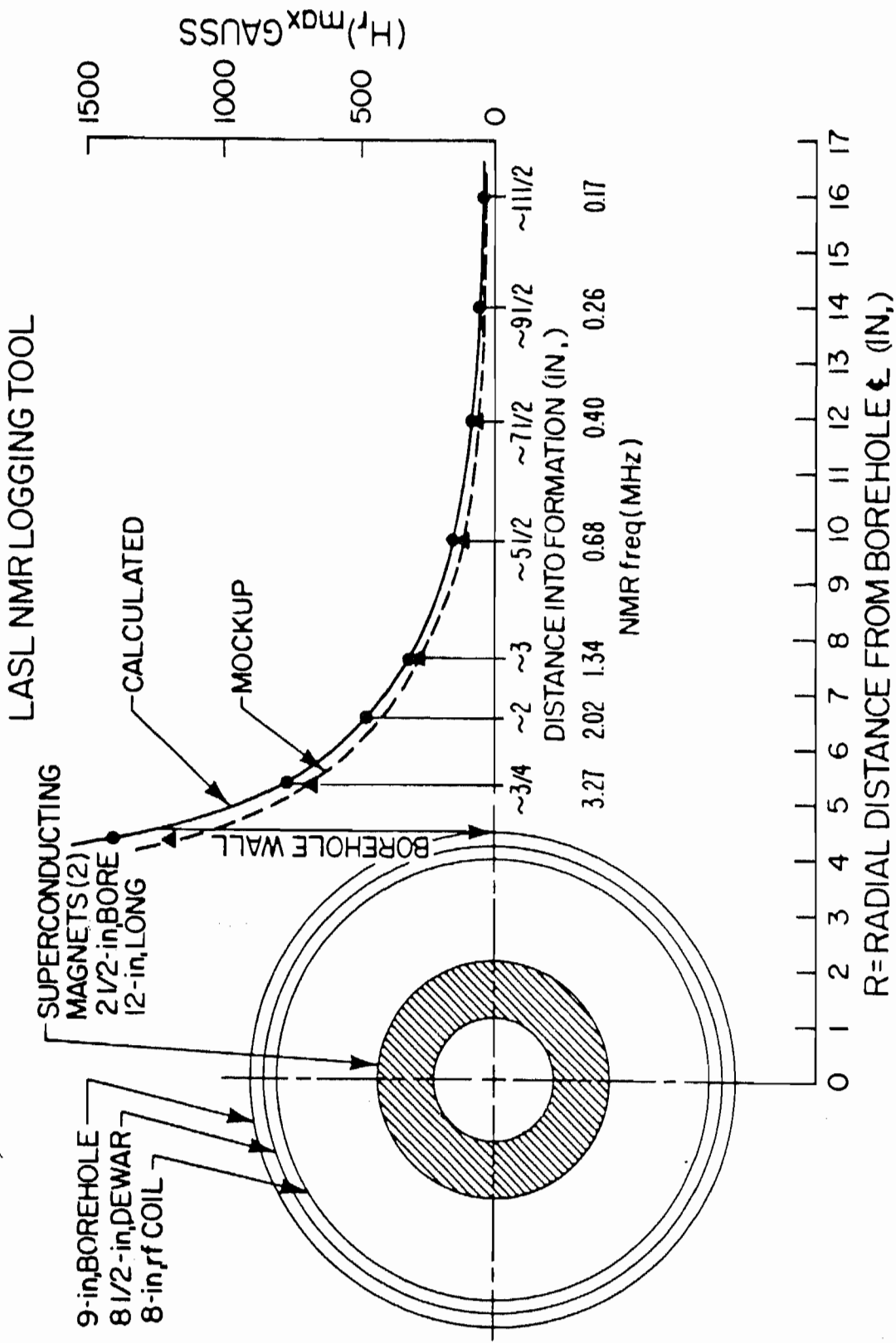


Fig. 21. Projected performance of logging tool using superconducting magnets.

For example, from Fig. 21 at $R = 11.93$ in.:

$$H_r = 94 \text{ G}, f = 0.4 \text{ MHz},$$

$$(S/N) = 4.5 \times (5.51/11.93)^2 \times (0.40/0.50)^2 = 0.61 \text{ in } 18 \text{ s}.$$

Then calculate S/N for other times using the relation,

$$(S/N)_2 = (S/N)_1 \sqrt{T_2/T_1}.$$

For example, to calculate the S/N expected in 1 s instead of 18 s,

$$(S/N)_1 = (S/N)_{18} \sqrt{1/18} = 0.61 \times 1/4.24 = 0.14.$$

VII. PROJECTED IMPROVEMENTS

The electromagnetic experiments were conducted under far from ideal conditions and the following estimates of predicted improvements in S/N were applied.

It is believed that because of field inhomogeneity around the torus, only ~25 per cent of the torus was effective in producing a signal. This deficiency will be corrected in a working tool. A factor of 4 was applied to account for the expected increase.

The noise level is quite high and far from optimum. It is estimated that about one-half the observed noise was due to a 60-Hz pickup and will be eliminated in a carefully designed tool. A factor of 2 was applied.

The remaining noise could be reduced through careful design. In particular, the use of superconducting magnets offers the possibility of dramatic reduction in noise levels because of the presence of cryogenic fluids to cool the magnets. If all the noise were thermal noise in the electronic devices, then the S/N reduction would be expected to vary as $1/T$; i.e., $S/N \propto 300/4 = 75$ or an increase in a factor of 75 (in S/N) in going from room temperature to 4 K of liquid helium.

A conservative estimate of the S/N gain to be expected would be to assume that the noise decreases as ΔT instead of T . This results in $(S/N)_{\Delta T} = \sqrt{300/4} = \sqrt{75} = 8.7$. For ease of calculation, a factor of 10 was applied. It should be pointed out, however, that the presence of liquid helium may make it possible to take advantage of the enormous gain in sensitivity of modern quantum interference devices (SQUIDS) to gain a larger increase in S/N than is included in the conservative procedure above. This possibility is being investigated.

The result of these factors is given in Table II. The signal integration time for a given S/N at a particular depth is shown in Fig. 22. For example,

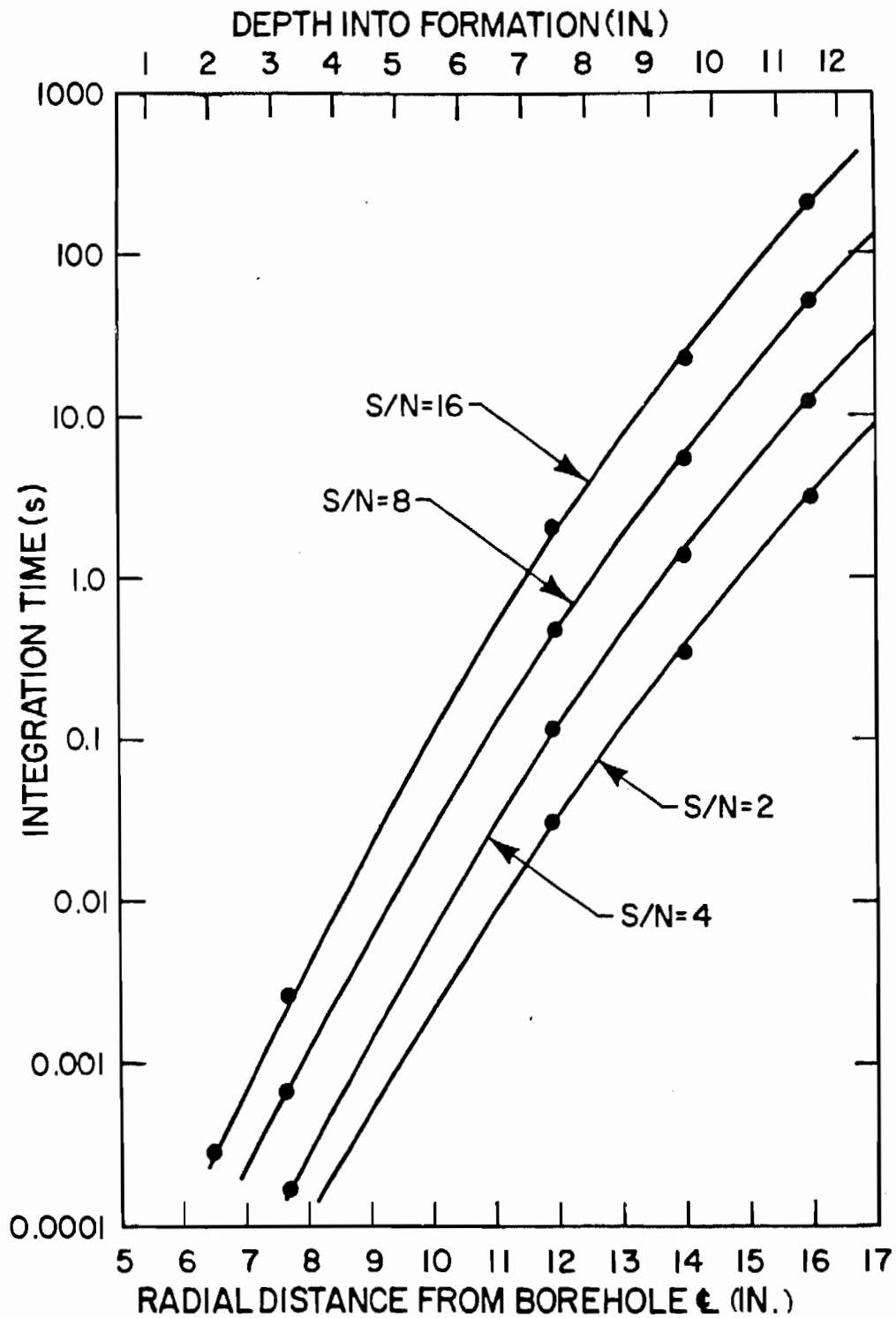


Fig. 22. Calculated integration time to achieve given S/N at selected depth into formation utilizing optimized electronics and superconducting magnets.

to obtain $S/N = 2$ at 7 1/2 in. into the formation, requires 3 s. These figures are for a porosity of 100 per cent. To find the integration time for the same (S/N) for a porosity of P, multiply by $(1/P)^2$. As an example,

$$\text{For } P = 0.20, T = 3 \text{ s} \times (1/P)^2 = 3 \times (5)^2 = 3 \times 25 = 75 \text{ s.}$$

A factor that has not been included is the correction for the ratio (R/a) when extrapolating from the 4-in. electromagnet to the superconducting magnet with a 2 1/2-in. bore. The effective diameter (~ about average diameter of windings) of the superconducting magnet was taken to be 3 in. in the calculations. The correction comes about because the width R of the "resonance" magnet. The toroidal area will be larger by $(4/3)^2 = (1.33)^2 = 1.78$, and the S/N will be 78 per cent larger with the superconducting magnet. This factor has not been included in the above calculations and therefore provides a conservative cushion to the estimates.

VIII. SUMMARY FY 79 ACCOMPLISHMENTS IN NMR

- A method for remotely producing a region of homogeneous magnetic field was conceived. Involved in this were the computer calculations on field strength and distribution and the confirmation of these calculations by laboratory measurements.
- The remote NMR detection was demonstrated for liquids (1) confined to toroidal sensitive region, (2) including, but not confined to, sensitive region, and (3) in pores of simulated rock.
- The NMR sensitivity vs distance from axis was measured.
- The data for projected performance of logging tool using super conducting magnets was extrapolated.
- A fracture strike mapping technique was conceived.

REFERENCES

1. Following completion of this work, the following work was called to our attention, in which Dr. Cook also describes the homogeneous region of radial magnetic field. John C. Cook, "Electromagnetic Resonance Borehole Assay Logging," Bu Mines OFR-69-78 (PB-283734)(1980).
2. J. R. Pierce, Theory and Design of Electron Beams (D. Van Nostrand Company, Inc., Princeton, New Jersey, 1954) p. 4.
3. D. I. Hoult, "Fast Recover, High Sensitivity NMR Probe and Preamplifier for Low Frequencies," Rev. Sci. Instrum. 50(2), 193 (1979).